

A RAKE PROCESSOR  
FOR THE  
IDENTIFICATION OF  
FADING COMMUNICATION CHANNELS

A thesis submitted  
in partial fulfilment of the requirements  
for the degree of  
MASTER OF TECHNOLOGY IN ELECTRICAL ENGINEERING

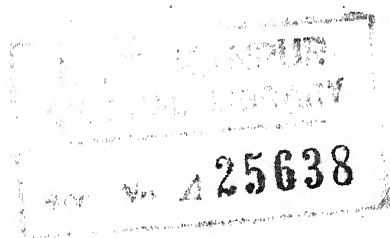
by

L. SUDHAKARA RAO

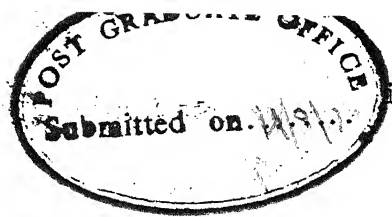
to the

DEPARTMENT OF ELECTRICAL ENGINEERING  
INDIAN INSTITUTE OF TECHNOLOGY, KANPUR

August, 1973



1976



CERTIFICATE

Certified that this work, 'A RAKE Processor for the Identification of Fading Communication Channels' by Mr. L. Sudhakara Rao has been carried out under my supervision and that this has not been submitted elsewhere for a degree.

*P. Ramakrishna Rao*

Dr. P. RAMAKRISHNA RAO  
ASSISTANT PROFESSOR  
DEPARTMENT OF ELECTRICAL ENGINEERING  
I.I.T., KANPUR

4 August, 1973

ACKNOWLEDGEMENTS

I express my deep sense of gratitude and appreciation to my guide Dr. P.R.K. Rao who, in large measure, spared his precious time in critical moments, supervised, stimulated and encouraged this project work.

L. SUDHAKARA RAO

CONTENTS

Page No.

Synopsis	..	..	iv
1. INTRODUCTION	..	..	1
1.0 Troposcatter as a Communication Channel	..	..	1
1.1 Need for Identification of Channel Characteristics	..	..	1
1.2 Characterization of Troposcatter Channel	..	..	3
1.3 Proposed Scheme of Channel response Identification	..	..	5
1.4 Outline of various Chapters	..	..	9
2 SYSTEM DESCRIPTION	..	..	11
2.0 Introduction	..	..	11
2.1 System Description	..	..	11
2.2 Quantization and Sampling	..	..	16
2.3 Data Analysis	..	..	18
3 CIRCUIT DESCRIPTION AND DESIGN	..	..	19
3.0 Introduction	..	..	19
3.1 Signal Attenuator	..	..	19
3.2 Noise Generator	..	..	31
3.3 Linear Addition of Signal and Noise	..	..	35
3.4 IF Amplifier	..	..	40
3.5 Multiplier	..	..	49
3.6 Video Amplifier	..	..	53
3.7 Polarity Sensing Detector	..	..	56
4 MECHANICAL CONSTRUCTION AND LAYOUT	..	..	63
4.0 Printed Cards	..	..	63
4.1 Mechanical Construction and Layout	..	..	64
4.2 Controls	..	..	64
5 PERFORMANCE MEASUREMENT AND CONCLUSIONS	..	..	67
APPENDIX-A : Brief Manufacturer's Specifications of the Devices	..	..	78
REFERENCES	..	..	79

## SYNOPSIS

The characterization and identification of fading communication channels such as a Troposcatter channel are usually a pre-requisite for using the medium for signal transmission by optimal modem techniques to combat multipath fading characteristics exhibited by such channels. A fading communication channel can often be adequately characterized by a linear system with an equivalent low-pass impulse response that is a complex Gaussian process.

(i) RAKE technique involves the use of wide band signalling at the transmitter and correlation reception at receiver as an anti-multipath measure over fading communication channels. By using correlation detection technique, the transmitted signal arriving with different time delays can be isolated. RAKE concept may also be applied for probing the Troposcatter channel to get estimates of channel response for different time delays.

Though the impulse response function  $g(t, \xi)$  of the channel is considered as continuous in both time,  $t$  and delay variable,  $\xi$  it can be considered <sup>known</sup> ~~for~~ practical point of view to be not finer than the inverse of the bandwidth,  $B$  of the sounding signal for identifying its estimates for different time delays. In view of the above, the fading channel can be represented by a tapped-delay line with number

of taps equal to the number of discrete paths with tap spacing corresponding to  $1/B$  which is referred to as multipath resolution. In such <sup>an</sup> tapped-delay line, the incoming signal appears at the input of delay line and after weightages called tap-gain functions which are random processes, the sum of the tap outputs constitutes the received signal at the receiver.

For anti-multipath signalling, a wide band-pass noise-like waveform such as PN sequence is a useful continuous signal structure. The waveform is a random process and a moderately long segment of such sequence exhibits <sup>preferable</sup> auto-correlation properties. Also, for cross-correlation purpose at receiver, an exact replica is available.

For channel response identification, the shifted replicas of the transmitted signal are generated for different values of time delays and then cross-correlated with the received signal. Because of the correlation property of the transmitted PN sequence, the outputs of the cross-correlators give the direct measure of apparent channel response at relative time delays.

(ii) The objective of the present system is to obtain the estimates of randomly varying quadrature components of channel response function for different time delays and then investigate the fluctuations caused by fading in signal phase and signal amplitude. At the transmitter, for probing

the medium, PN sequence of period  $(2^{15}-1)$  is chosen by which the 60 MHz IF is phase-shift keyed at 10 M bauds and then filtered to 10 MHz bandwidth to be transmitted over Troposcatter channel. At receiver, the received signal is split into in-phase and quadrature components which are cross-correlated with identical binary streams each of which is delayed by 0.1  $\mu$ sec with respect to the preceding one. This provides a multi-path resolution of 0.1  $\mu$ sec. The outputs of the cross-correlators give the estimates of the randomly varying quadrature components of channel response function for different time delays.

(iii) The hardware realization of a part of the receiver system as shown in block diagram of Fig.3.0 includes the addition of Gaussian noise of 10 MHz bandwidth and centred at 60 MHz to the incoming 60 MHz IF signal, splitting of the signal into in-phase and quadrature components followed by extraction of the video components and conversion of the positive or negative going signal into digital '1' or '0' in polarity sensing detectors.

## CHAPTER - 1

### INTRODUCTION

#### 1.0 TROPOSCATTER AS A COMMUNICATION CHANNEL:

The Troposphere is the region of earth's atmosphere extending from ground to a height of about 10 KM. The turbulent air motion and water content cause variations in the refractive index of Troposphere from point to point as well as in time. In one model, the changes in refractive index are grouped in 'blobs' in earth's atmosphere which represent refractive indices different from that of the surrounding medium. This abrupt change in refractive index causes a 'scattering' of EM wave and thus the energy is re-radiated towards the earth by blob. The scatter radiation comes from the large number of scatterers within the volume common to both transmitting and receiving antenna beams.

Troposcatter provides (a) multichannel service over distances of 100 KM to 1000 KM, (b) good spectrum utilization and (c) high degree of security.

#### 1.1 NEED FOR IDENTIFICATION OF CHANNEL CHARACTERISTICS:

Characterization and identification of fading communication channels are normally required for using such media for transmitting signals by optimal modem techniques. In this section, the nature of propagation

vagaries like fading and multipath are described which demand channel characterization.

Considering the transmission of continuous tone (carrier) from the transmitter, let  $n$  be the number of blobs contributing to the received signal which can be treated as a random variable. Also, the amplitude  $A_i(t)$  and phase  $\phi_i(t)$  of the received signal from each of these blobs can be treated as random variables.

In terms of random phasors, the resultant amplitude,  $R(t)$  and phase,  $\theta(t)$  of the signal at receiver antenna can be represented by

$$R(t) e^{j\theta(t)} = \sum_{i=1}^n A_i(t) e^{j\phi_i(t)} \quad (1.1)$$

Considering independently varying large number of random phasors, the values of the quadrature components of the resultant at any instant are uncorrelated and approach independently as Gaussian variables. The resulting sum at any instant has the characteristics of a narrow band-pass Gaussian noise with Rayleigh fading envelope and uniformly distributed phase. In Eq. (1.1), the amplitude of the resultant signal  $R(t)$  has Rayleigh distribution and phase  $\theta(t)$  is uniformly distributed over  $(0, 2\pi)$ .

$$p_R(r) = \frac{r}{\sigma^2} e^{-r^2/2\sigma^2}, \quad r \geq 0$$

$$p_\theta(\theta) = 1/2\pi, \quad 0 \leq \theta \leq 2\pi$$

Where  $\sigma^2$  is the variance of independent and identically distributed zero-mean normal random variables,  $X(t)$  and  $Y(t)$  (real and imaginary components of phasor  $R(t) e^{j\theta(t)}$ ).

To introduce a more quantitative expression to the channel descriptions above, it is necessary to characterize the channel response function and discuss covariance functions in statistical model of fading.

## 1.2 CHARACTERIZATION OF TROPOSCATTER CHANNEL:

The tropochannel may be characterized as a linear time-varying band-pass filter whose impulse response varies stochastically as a Gaussian process. If  $Z(t)$  is the complex low-pass signal input and  $g(t, \xi)$  is the complex equivalent low-pass impulse response of such filter, then the complex low-pass signal output can be represented as

$$w(t) = \int_{-\alpha}^{\alpha} g(t, \xi) z(t - \xi) d\xi \quad (1.2)$$

If short term fading characteristics exhibit Rayleigh distribution, then  $g(t, \xi)$  and hence  $w(t)$  is a zero-mean complex Gaussian process in  $t$  with its quadrature components having the same variance for each  $t$ . If  $z(t) \leftrightarrow z(f)$ ,

$$z(t - \xi) = \int_{-\alpha}^{\alpha} z(f) e^{j2\pi f(t - \xi)} df \quad (1.3)$$

Letting  $g(t, \xi) \longleftrightarrow T(t, f)$ , from Eqs. (1.2) and (1.3),

$$w(t) = \int_{-\alpha}^{\alpha} T(t, f) z(f) e^{j2\pi ft} df \quad (1.4)$$

where  $T(t, f)$  is the time-variant transfer function of the channel and is also a zero-mean complex Gaussian process.

Correlation functions:

The Tropo-channel can adequately be characterized by at least 2nd order statistical functions the measurement of which requires that the process should be at least wide-sense stationary over time intervals of the order of measurement time.

Considering the mean of  $g(t, \xi)$  as zero and  $g(t, \xi) d\xi$  as the complex gain associated with path delays in the interval  $(\xi, \xi + d\xi)$ , the correlation function  $Q(\xi, \eta, \tau)$ , is called Tap-gain or Path-gain Correlation function or Multipath Time-covariance function of WSS channel.

$$Q(\xi, \eta, \tau) = \overline{g^*(t, \xi) g(t + \tau, \eta)} \quad (1.5)$$

For a WSS channel which also exhibits uncorrelated scattering (WSSUS),  $Q(\xi, \eta, \tau)$  has the form

$$Q(\xi, \eta, \tau) = Q(\xi, \tau) \delta(\xi - \eta)$$

$Q(\xi, 0)$  is called the Delay power spectrum or Multipath intensity profile. For WSSUS channels, scattering function  $S(\xi, \psi)$  is defined as

$$S(\xi, \psi) = \int Q(\xi, \tau) e^{-j2\pi\psi\tau} d\tau \quad (1.6)$$

$S(\xi, \mathcal{D})$  describes the relative intensity of all scatterers involving a propagation path of relative delay  $\xi$  and having a Doppler Shift  $\mathcal{D}$ .

### 1.3 PROPOSED SCHEME OF CHANNEL RESPONSE IDENTIFICATION:

#### 1.3.1 Introduction:

In this section, a tapped-delay-line representation for the channel has been discussed. The impulse response function of the channel,  $g(t, \xi)$  is considered as containing a continuous multipath structure over a continuum of values of  $\xi$ . Practically, this continuum working is impossible. However, we can expect that the detail considered for estimating  $g(t, \xi)$  need not be finer than  $1/B$  where  $B$  is bandwidth of the sounding signal.

The signal received over a fading multipath channel can be represented as

$$w(t) = \int_{-\alpha}^{\alpha} g(t, \xi) z(t - \xi) d\xi \quad (1.7)$$

where  $w(t)$  and  $z(t)$  are the complex envelopes of the received and transmitted waveforms respectively and  $g(t, \xi)$  is the time-varying equivalent low-pass impulse response of the channel. Variations of  $g(t, \xi)$  as  $t$  varies are slow so that the dependence of  $g(t, \xi)$  on  $\xi$  can be found by means of sounding signal.

### 1.3.2 Tapped-delay-line representation for the channel:

Let the complex envelope of the transmitted signal,  $z(t)$  has a 2-sided spectrum such that  $-\frac{B}{2} \leq f \leq \frac{B}{2}$ . From sampling theorem,  $z(t)$  can be expressed as

$$z(t) = \sum_{j=-\alpha}^{\alpha} z(j/B) (\sin \pi B(t-j/B) / \pi B(t-j/B)) \quad (1.8)$$

From Eqs. (1.7) and (1.8), it can be shown that

$$w(t) = (1/B) \sum_{j=-\alpha}^{\alpha} g_1(t, j/B) z(t-j/B), \quad (1.9)$$

where  $g_1(t, j/B)$  is an equivalent low-pass time varying impulse response for the channel corresponding only to its low-pass transfer function over  $-B/2 \leq f \leq B/2$ . Only that portion of the channel response which is relevant to transmitted signal confinement of  $|f| < B/2$  is considered.

For signals bandlimited to  $B$ , it is enough if the behaviour of the channel is estimated in terms of effective impulse response  $g_1(t, \xi)$  at intervals spaced  $1/B$  apart in  $\xi$ . Letting  $g_1(t, j/B) = g_j(t)$ , the channel model implied by Eq. (1.9) is given within dotted lines of Fig.1.1.

### 1.3.3 Channel response identification:

The present scheme of identifying the channel response is the use of wideband signalling and correlation

reception as an antimultipath measure over fading channels. For sounding the channel, a wide band-pass noise-like waveform (PN sequence) is a useful continuous signal structure. An exact replica is also available as cross-correlation reference and a moderately long segment of such sequence exhibits autocorrelation properties. Let a segment of length  $T$  of PN sequence be used as sounding signal over interval  $0 < t \leq T$  ( $T \gg 1/B$ ).

The estimates of  $g_j(t)$  can be obtained by extracting an identical  $T$ -length segment of the replica process available at receiver, delaying it by  $K/B$  and cross-correlating it against the received signal,  $w(t)$ . Letting  $j/B = \xi_j$  and  $K/B = \eta_k$ , the output of cross-correlator may be given as

$$\begin{aligned}
 s_k(t) &= \int_{\eta_k}^{T+\eta_k} w(t) z^*(t-\eta_k) dt \\
 &= 1/B \sum_{j=-\alpha}^{\alpha} g_j(t) \int_{\eta_k}^{T+\eta_k} z^*(t-\eta_k) z(t-\xi_j) dt \quad (1.11)
 \end{aligned}$$

If  $T \gg 1/B$ , we can assume that the finite length integral can be well approximated by its average over ensemble of all possible  $T$ -length segments of  $z(t)$ .

$$\phi(\xi) = 1/T \int_0^T z^*(t) z(t+\xi) dt \quad (1.12)$$

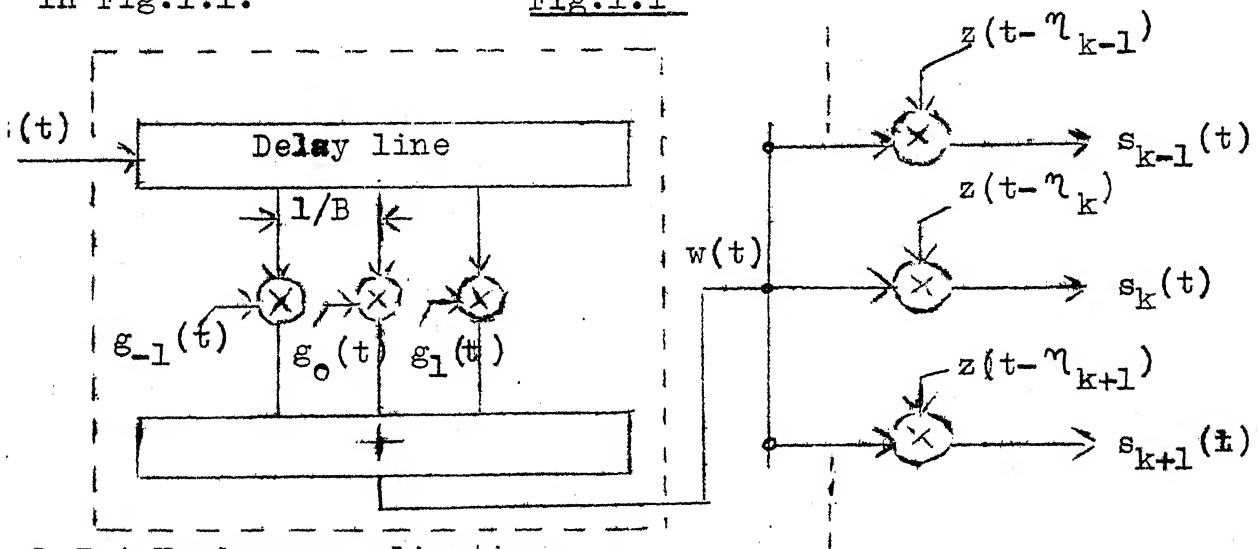
From Eqs. (1.11) and (1.12),

$$s_k(t) = T/B \sum_{j=-\alpha}^{\alpha} g_j(t) \phi_z(\tau_k - \xi_j) \quad (1.13)$$

Whenever  $\tau_k = \xi_j$ ,  $s_k(t)$  is maximum because of choice of  $z(t)$ . Thus the output of cross-correlator,  $\phi_z(0) g_j(t)$  is the estimate of  $g_j(t)$ . So, the correlation with reference relatively delayed by  $\tau_k = K/B$  selects only that part of the arriving signal energy represented by Kth tap in the tapped delay line model of the channel.

The block diagram implied by the tapped-delay - line model of multipath fading channel and correlation reception to measure channel response for different time delays is shown in Fig.1.1.

Fig.1.1



#### 1.3.4 Hardware realization:

The block diagram shown in Fig.3.0 represents the designed and fabricated part of the receiver system. The incoming 60MHZ IF signal is added with locally generated Gaussian noise of 10 MHZ bandwidth and centred at 60 MHZ so

as to maintain required S/N ratio to linearize the polarity sensing process. It is then fed to two multipliers the other inputs of which being the quadrature components of local 60 MHz IF which is in phase with the transmitted IF. Thus, the incoming signal is split into normal (in-phase) and quadrature components. The outputs of the multipliers are passed through low pass filters to extract the video components which are amplified by video amplifiers to be fed to polarity sensing detectors represented by difference-amplifier and comparator circuits. The output of a polarity sensing detector is a logical '1' or '0' for positive or negative going signal component.

The resulting in-phase and quadrature components of the incoming signal are to be cross-correlated with the time-shifted replicas of the transmitted signal (PN sequence) to get estimates of channel impulse response function for different time-delays.

#### 1.4 OUTLINE OF VARIOUS CHAPTERS:

Chapter 1 gives a brief discussion of fading troposcatter channel characteristics followed by tapped-delay line model of representing channel and the proposed scheme of channel response identification.

Chapter 2 mostly deals with functional system block diagram based on the technique of channel response identification as discussed in Chapter 1.

Chapter 3 contains starting with block diagram of the fabricated part of the proposed system, both a description and the design of different circuits involved.

Chapter 4 gives information about printed cards and mechanical construction and layout details of the boxes alongwith description and purpose of the provided controls.

In Chapter 5, a brief description of tests carried out and the experimental results obtained have been given.

## CHAPTER - 2

### SYSTEM DESCRIPTION<sup>10,11,12</sup>

#### 2.0 INTRODUCTION:

RAKE technique of wideband signalling and correlation reception is used for communication over fading channels. This technique can also be used for probing the troposcatter channel to get an estimate of channel scattering function.

#### 2.1 RAKE SYSTEM DESCRIPTION:

##### 2.1.1 System Objective:

The objective of the system is to record randomly varying in-phase and quadrature components of channel response function,  $g(t, \xi)$  as it varies both in  $\xi$  and  $t$  and analyse the data obtained to provide an estimate of the channel scattering function.

##### 2.1.2 System Characteristics:

(a) Operating frequency	.. 2.1 GHZ
(b) Transmission technique	.. AM
(c) IF frequency	.. 60 MHZ
(d) Sounding Signal	.. PN sequence (period = $2^{15}-1$ )
(e) Method of signal modulation	.. PS Keying at 10 Mega bauds
(f) Signal bandwidth	.. 10 MHZ
(g) Multipath resolution	.. 0.1 $\mu$ sec.

<del>(h)</del> Order of diversity	... <del>15</del>
<del>(i)</del> Diversity technique	... Multipath
<del>(j)</del> Detection technique	... Correlation
<del>(k)</del> Mode of propagation	.. Single hop, overland scatter
(l) Test-link range	.. 300 miles
<del>(m)</del> Integration time	.. <del>millisec.</del>

### 2.1.3 Signalling:

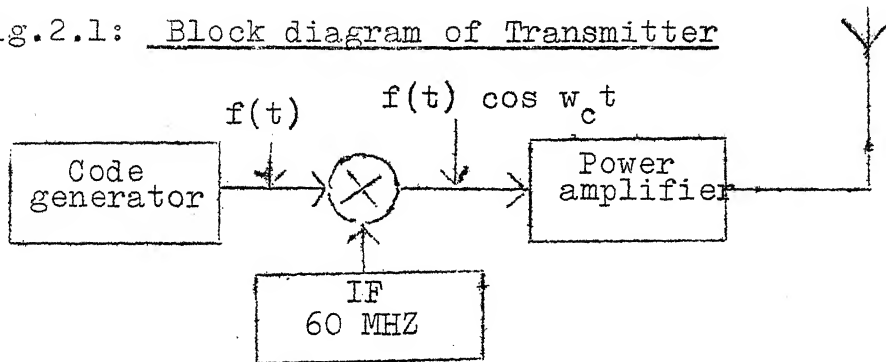
To probe the medium for its impulse response, wideband signalling is required. Pulses of very short duration are unsuitable as the repetition rate cannot be made low enough to keep the observed response from overlapping in time due to limitation of peak power than can be transmitted. However, a wideband noise like waveform i.e., Pseudo-Noise sequence (PN Seq.) serves as an excellent continuous signal structure. It contains sufficient details so that the waveform at one instant of time can be distinguished from that at another instant of time. (since, at zero time-lag, auto-correlation =  $2^M - 1$  and at time lags of one or more elements, auto-correlation = 0 or unity where M is the number of stages in shift register generating PN sequence).

### 2.1.4 Simplified block diagram of Transmitter:

The code generator in Fig.2.1 is a 15-stage shift register connected with feedback for maximal length code generation. The IF is 60 MHz phase-shift keyed at 10 M bauds by PN sequence, filtered to 10 MHz bandwidth and then power

amplified to be transmitted over a tropospheric path.

Fig.2.1: Block diagram of Transmitter



#### 2.1.5 Block diagram of Receiver:.

Block diagram of RAKE receiver is shown in Fig.2.2. The transmitted signal is corrupted with additive white gaussian noise and arrives at the receiver sequentially via different paths of the illuminated common volume of the troposcatter medium.

The multiplied output of frequency synthesizer is used as receiver local oscillator. The resultant 60 MHz IF signal of 10 MHz BW serves as an input to the signal attenuator stage of RAKE demodulator.

Locally generated gaussian noise with 10 MHz BW and centred at 60 MHz is added to IF signal so as to maintain required S/N ratio to linearize the polarity sensing process (see section 2.2).

The signal is then fed to IF amplifier the output of which is injected into two multipliers of normal and quadrature channels. The quadrature components of the locally derived 60 MHz IF which is in phase with transmitted IF serve as other inputs to the multipliers.

The low-pass filters recover the required normal and quadratic components of sounding signal by eliminating the high frequency content of multiplier outputs.

The video outputs are then amplified and fed to polarity sensing detectors (PSD). Each PSD is strobed by 10 MHZ master clock and at the moment of strobing, PSD output is a logical '1' or '0' depending upon whether the input signal is positive or negative in polarity.

The receiver contains a shift register to generate a PN Seq. which is identical and in synchronism with the one used at the transmitter. Synchronization of PN sequence can be provided in the synchronous sweep circuit.

The shift register provides 15 time-shifted and sequenced local copies of transmitted PN code which are cross-correlated with the sampled normal and quadratic components of received signal in 30 mod-2 adders to get a continuous estimate of amplitude and phase for each particular delay/tap.

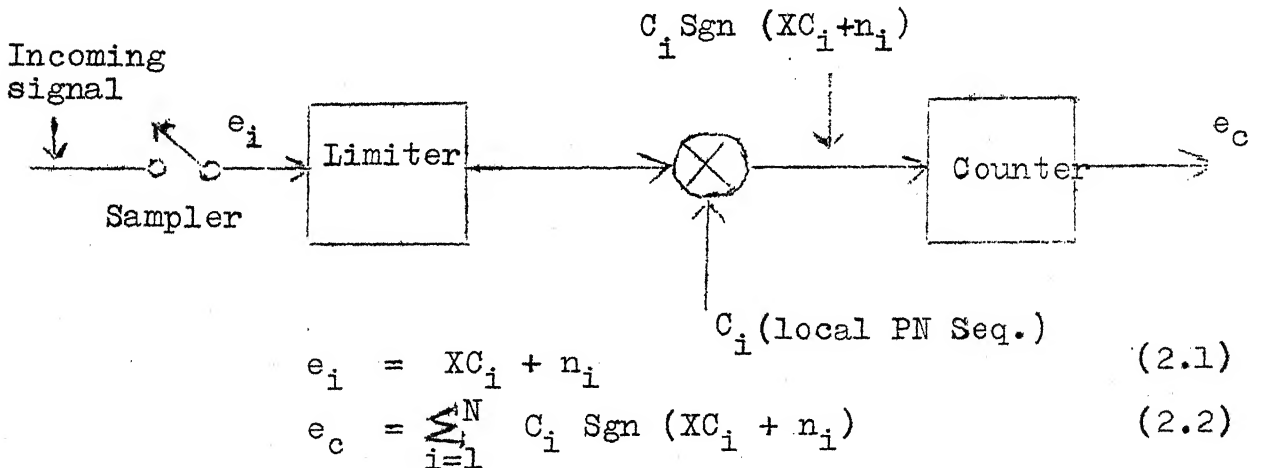
The storage counter provided for each tap accumulates the information of how many times the signal and code sequence correlate during each integration period. At the end of integration period, storage counter is reset to zero after its selected number of active bits are transferred into a buffer register.

The outputs of buffer register are then multiplexed and recorded on a digital tape recorder for computer processing.

## 2.2 QUANTIZATION AND SAMPLING<sup>10</sup>:

The one-bit quantization or limiting of the input samples will introduce an error causing nonlinearity between the average counter output and input signal component. Anyhow, the amount of error can be minimized by adding an appropriate amount of Gaussian noise to the received signal. Let  $e_i$  be the output of the sampler and input to one of the quadrature quantizers and  $e_c$ , the output of the counter as shown in Fig.2.3.

Fig. 2.3



where  $X$  = one quadrature component of channel gain at one particular delay and is assumed constant over an integration period,

$C_i$  = transmitted PN sequence =  $\pm 1$ ,

$n_i$  = samples of (a) received noise and  
(b) signals with delays differing by more than a bit period of PN seq. which is negligible,

$$\text{Sgn}(XC_i + n_i) = \begin{cases} = +1 & \text{for } (XC_i + n_i) \text{ positive} \\ -1 & \text{for } (XC_i + n_i) \text{ negative} \end{cases}$$

By carrying out multiplication process before limiter,

Eq.(2.2) is mathematically equivalent to

$$e_c = \sum_{i=1}^N \text{Sgn}(X+n_i) = \sum_{i=1}^N \text{Sgn}(X+n_i) \quad (2.3)$$

where  $n_i$  has same properties as  $n_i$ ,

$X$  is constant over integration period,

$$\text{Sgn}(X+n_i) = \begin{cases} +1 & \text{with probability } P \\ -1 & \text{with probability } (1-P) \end{cases}$$

$$P = \Pr [X > -n_i] = \left[ \frac{1}{\sqrt{2\pi}\sigma} \right] \int_{-X}^{\infty} e^{-y^2/2\sigma^2} dy$$

$$= \frac{1}{2} + (1/\sqrt{2\pi}) X/\sigma \quad \text{for small S/N ratio} \quad (2.4)$$

(i.e.,  $X \ll \sigma$ ) at limiter

using Eqns. (2.3) and (2.4),

$$(a) \text{ Mean of counter output, } : \bar{e}_c = N \sqrt{2/\pi} X/\sigma \quad (2.5)$$

Eq.(2.5) ensures linearity of counter output to input

signal component by adding an appropriate amount of

Gaussian noise to the received signal preceding the limiter

and sampler.

(b) With constant signal and independent noise from sample to sample, variance of counter output,  $\sigma_c = N$ . (2.6)

(c) RMS S/N ratio of counter output,  $(S/N)_c = \sqrt{2N/\pi} \cdot (X/\sigma)$   
(2.7)

### 2.3 DATA ANALYSIS:

The outputs of cross correlators or RAKE taps can be considered as a set of estimates of  $g_j(t)$  where  $g$  is a complex number (phasor) represented by normal (in-phase) and quadrature components of tap output and  $j$  identifies the tap being considered.

Considering  $n$  observations and taking sample mean i.e., time averaging over a finite time of experiment, tap-gain correlation and scattering functions for different time delays/taps can be computed using Eqns. (1.4) and (1.5).

## CHAPTER 3

### CIRCUIT DESCRIPTION AND DESIGN

#### 3.0 INTRODUCTION:

In this chapter, the operation and hardware realization of the various circuits used are discussed. Except where considered necessary, the discussion has been limited to a brief presentation of the salient features.

A functional block diagram of the designed and fabricated part of the system is shown in Fig.3.0.

The incoming 60 MHz IF signal corrupted with additive White Gaussian Noise constitutes the input signal with a bandwidth of 10 MHz.

The binary sequences at normal and quad. output terminals are further processed in the digital correlator and counting circuits to obtain the estimates of the fading channel characteristics.

#### 3.1 SIGNAL ATTENUATOR <sup>1,2,5</sup>

##### 3.1.1 INTRODUCTION:

Conventional attenuators (i.e. ladder network and electronic attenuator using emitter follower) may be unsuitable at very high frequencies without good quality contact switches. Moreover, neutralization of stray and wiring capacitances may pose problems in these cases.

However, an FET used as a voltage controlled resistor (VCR) can serve as an excellent signal attenuator<sup>1</sup>. Such an attenuator can have a large dynamic range and adjustable bandwidth.

An FET in the region where the drain-source voltage  $V_{DS}$  is approximately zero may be shown<sup>17</sup> for any reverse bias  $V_{GS}$  between 0 and  $V_p$  to have a small signal drain-to-source resistance  $r_d$  to be a function of  $V_{GS}$  given by

$$r_d(V_{GS}) = r_d(0)/(1-K V_{GS})$$

where  $V_{GS}$  is the gate-source voltage,  
 $r_d(0)$  is the drain-to-source resistance at  
 $V_{GS} = 0$  and

$K$  is a constant dependent upon FET type

Thus, by controlling  $V_{GS}$ , a variable voltage-controlled resistor may be obtained.

### 3.1.2 CONFIGURATION SELECTION:

Of the two commonly used configurations shown in Figs.3.1 and 3.2, configuration-B is favoured as configuration-A has the following disadvantages.

- (a) The output of VCR has to be terminated into a 50-ohm load. As VCR appears in the low side of the attenuator,

Fig. 3.0 : Block Diagram of fabricated part of the system

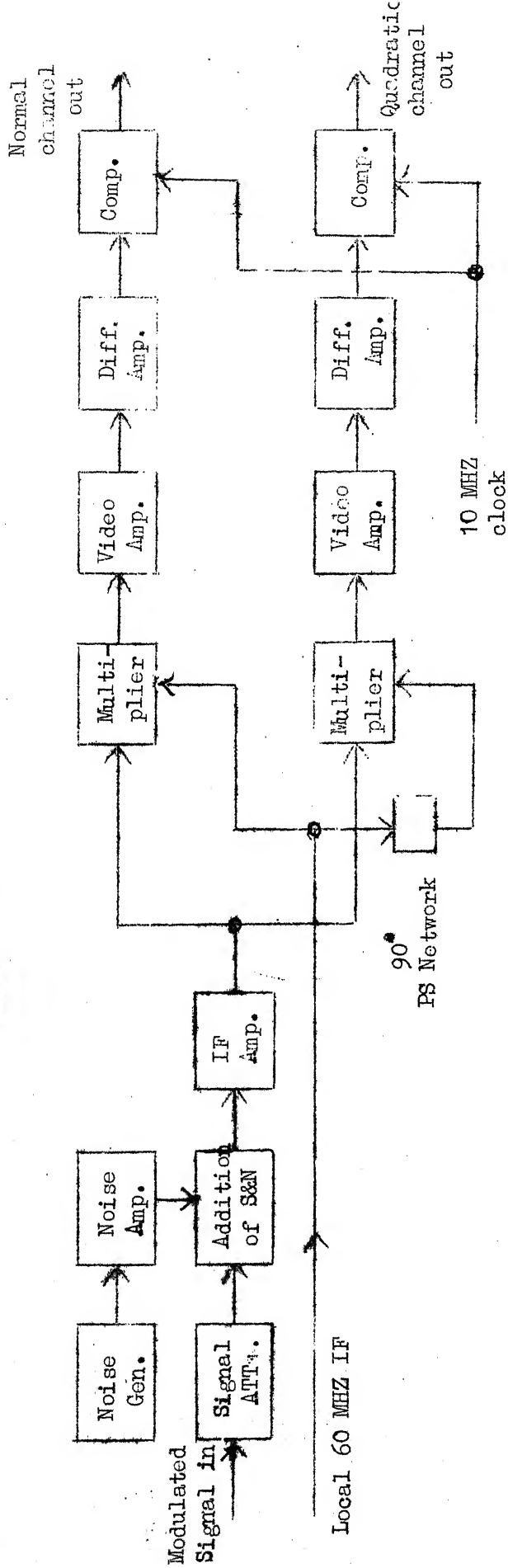


Fig. 3.1: CONFIGURATION-A

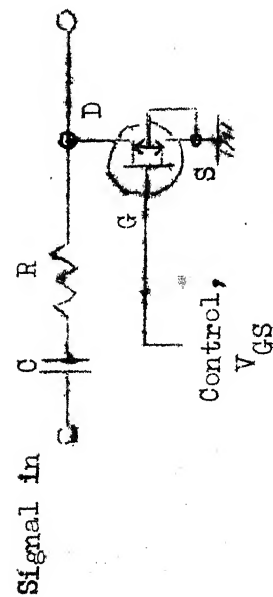
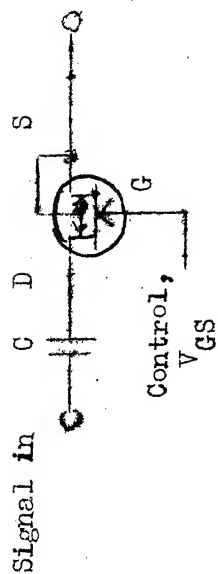


Fig. 3.2: CONFIGURATION-B



the following stage should have a very high input impedance.

(b) There is  $180^\circ$  phase shift between input and output.

(c) The input signal level should be high.

### 3.1.3 CIRCUIT CONFIGURATION:

The circuit configuration used for signal attenuation at 60 MHz range using FET is shown in Fig.3.3 and the equivalent high-frequency model is given in Fig.3.4.

Fig.3.3      Circuit Configuration

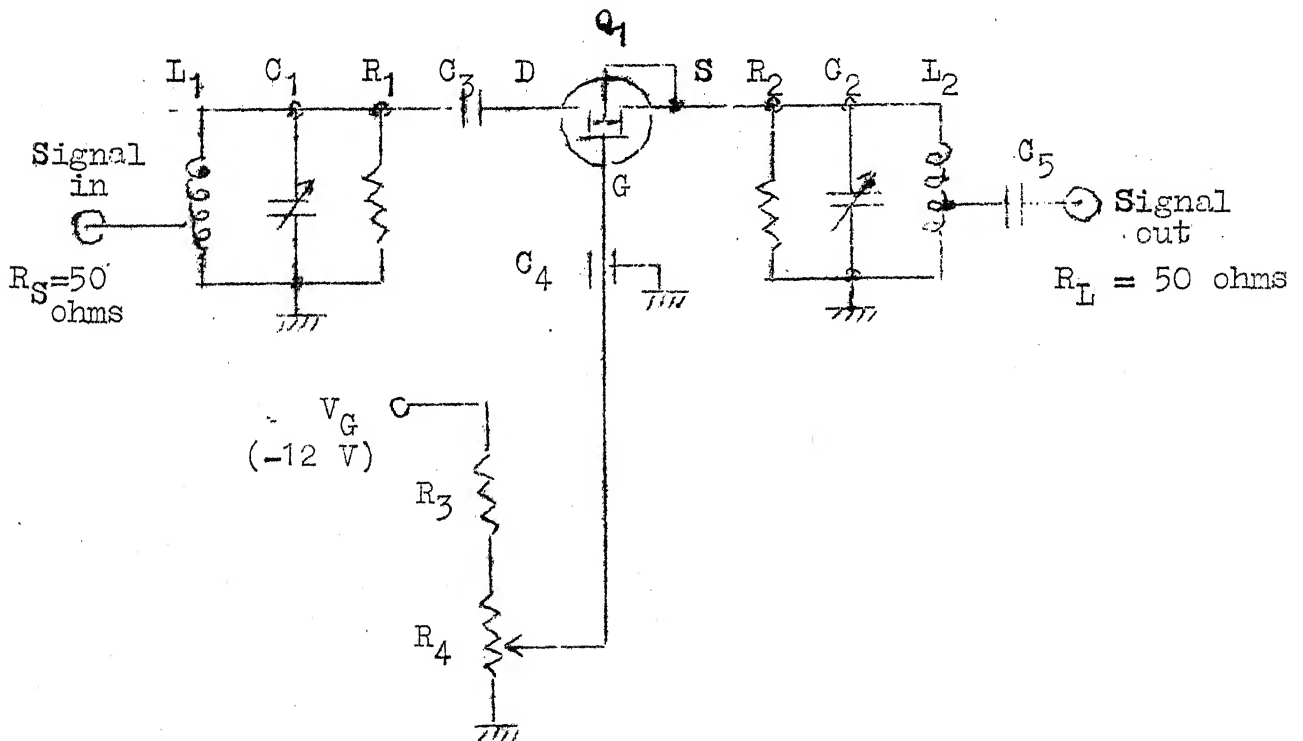
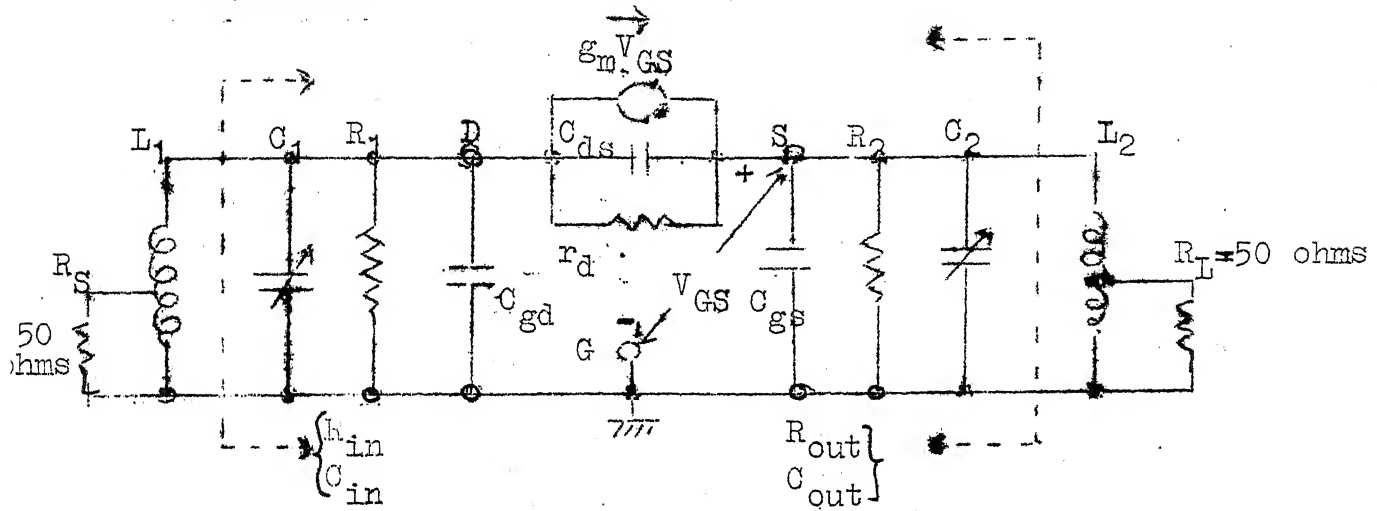


Fig.3.4: Equivalent high-frequency model of Fig.3.3



$C_{in}$  and  $L_1$  resonate at 60 MHZ

$C_{out}$  and  $L_2$  resonate at 60 MHZ

$V_{GS}$  is the test voltage

#### 3.1.4 DESIGN OBJECTIVES:

- 3.1.4.1 Frequency of operation : 60 MHZ
- 3.1.4.2 Band-width : 15 MHZ
- 3.1.4.3 Input impedance : 50 ohms
- 3.1.4.4 Output impedance : 50 ohms
- 3.1.4.5 Control voltage range,  $V_{GS}$ : 0 to -5 volts
- 3.1.4.6 Voltage attenuation range : -15 dB
- 3.1.4.7 Supply voltage available : -12V

#### 3.1.5 DESIGN CONSIDERATIONS:

- 3.1.5.1 A straight forward analysis of the equivalent circuit in Fig.3.4 would show that

$$\begin{aligned}
 R_{out} &\approx R_2 \parallel \frac{1}{g_m} && \text{for } r_d \gg R_1 \\
 C_{out} &= C_2 + C_{gs} + C_{ds}(\mu+1) + C_{stray} \\
 R_{in} &\approx R_1 && \text{for } r_d \gg R_1 \\
 C_{in} &= C_1 + C_{gd} + \frac{C_{gs}}{\mu+1} + C_{stray}
 \end{aligned}$$

### 3.1.5.2 Conditions to be satisfied:

- (a) For  $R_{out}$  to be less dependent on  $g_m$  variations,  
 $R_2$  should be as small as possible when compared to  $\frac{1}{g_m}$ .
- (b) For  $R_{out}$  to be less dependent on  $r_d$  variations,  $R_1$   
 should be as small as possible when compared to  $r_d$ .

Therefore, both  $R_1$  and  $R_2$  should be chosen as small as possible so as to keep  $R_{out}$  to be less dependent on  $g_m$  and  $r_d$  variations which occur due to varying  $V_{GS}$ . In such case

$$\begin{aligned}
 R_{out} &\approx R_2 \quad \text{and} \\
 R_{in} &\approx R_1
 \end{aligned}$$

### 3.1.6 SELECTION OF DEVICE AND COMPONENTS

3.1.6.1 Device chosen is Junction FET, type BFW10, n-channel.

Typical characteristics of BFW10 are as given in Appendix-A.

3.1.6.2 Resistors:  $R_1 = R_2 = 180 \text{ ohms}$

### 3.1.7 CIRCUIT DESIGN:

Centre frequency,  $f_o = 60 \text{ MHz}$

Bandwidth,  $B = 15 \text{ MHz}$

$$W_o = 2\pi f_o = 6.3 \times 60 \times 10^6 = 3.78 \times 10^8 \text{ radians}$$

$$\frac{1}{W_o} = 2.645 \times 10^{-9} \text{ rad}^{-1}$$

$$\text{Loaded } Q \text{ of tank circuit, } Q_L = \frac{f_o}{B} \quad (3.1)$$

$$= \frac{60}{15} = 4$$

### 3.1.7.1 Input Network:

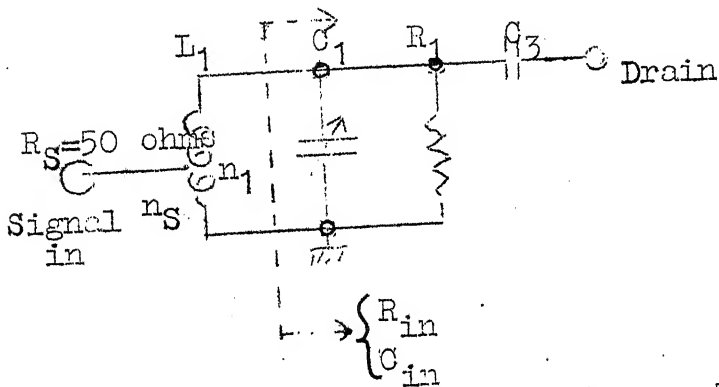


Fig. 3.5

Source resistance,  $R_S = 50 \text{ ohms}$

$$R_{in} = R_1 = 180 \text{ ohms}$$

Total capacitance shunting  $L_1 = C_{in} = C_1 + C_{stray} + C_{gd} + \frac{C_{gs}}{\mu+1}$

$R_S$  is reflected as 180 ohms onto the right hand side of  $L_1$  and across  $R_1$ . Therefore, for impedance matching, the effective resistance shunting  $L_1$  is

$$R_1' = \frac{R_1}{2} = \frac{180}{2} = 90 \text{ ohms}$$

$$L_1 = \frac{R_1'}{W_o Q_L} \quad (3.2)$$

$$= \frac{90 \times 2.645 \times 10^{-9}}{4} = 0.06 \mu\text{H}$$

For single-layer solenoids of the proportions normally used in radio work, the inductance is given to an accuracy of about 1 percent by an approximate formula<sup>6</sup>

$$L = \frac{n^2 r^2}{9r + 10l} \mu h \quad (3.3)$$

where  $L$  is the inductance in microhenries

$r$  is the radius of coil (inches) between the centres of conductors

$n$  is the number of turns

$l$  is the length of the coil (inches) i.e.,  $n$  times the distance between centres of adjacent turns.

For  $n = 4$  Turns,

$r = 0.276''$  (7 mm) and

$l = 0.4''$ ,

$L \approx 0.06 \mu h$ .

$$\begin{aligned} \text{Total capacitance across } L_1 \text{ is } C_{in} &= \frac{1}{W_o^2 L_1} \quad (3.4) \\ &= 115 \text{ pf.} \end{aligned}$$

Therefore, external capacitance required across  $L_1$  is

$$C_1 = 115 - (C_{\text{stray}} + C_{gd} + \frac{C_{gs}}{\mu + 1}) \text{ pf}$$

Experimentally,  $C_1$  is determined and found to be 97 pf

To find tap on  $L_1$ :

$$\begin{aligned} \frac{n_S}{n_1} &= \sqrt{\frac{R_S}{R_1}} \quad ; \quad n_S = n_1 \sqrt{\frac{R_S}{R_1}} \quad (3.5) \\ &= 2 \text{ turns from ground} \end{aligned}$$

3.1.7.2 Output Network:

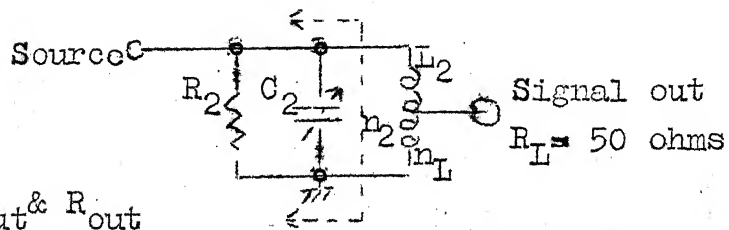


Fig. 3.6:

$$R_{out} = R_2 = 180 \text{ ohms}$$

$$C_{out} = \text{Total capacitance across } L_2$$

$$= C_2 + C_{stray} + C_{gs} + C_{ds} (\mu + 1)$$

$$L_2 = 0.06 \mu\text{H}$$

$$n_2 = 4 \text{ turns}$$

$$n_L = 2 \text{ turns from ground}$$

$$C_{out} = 115 \text{ pf}$$

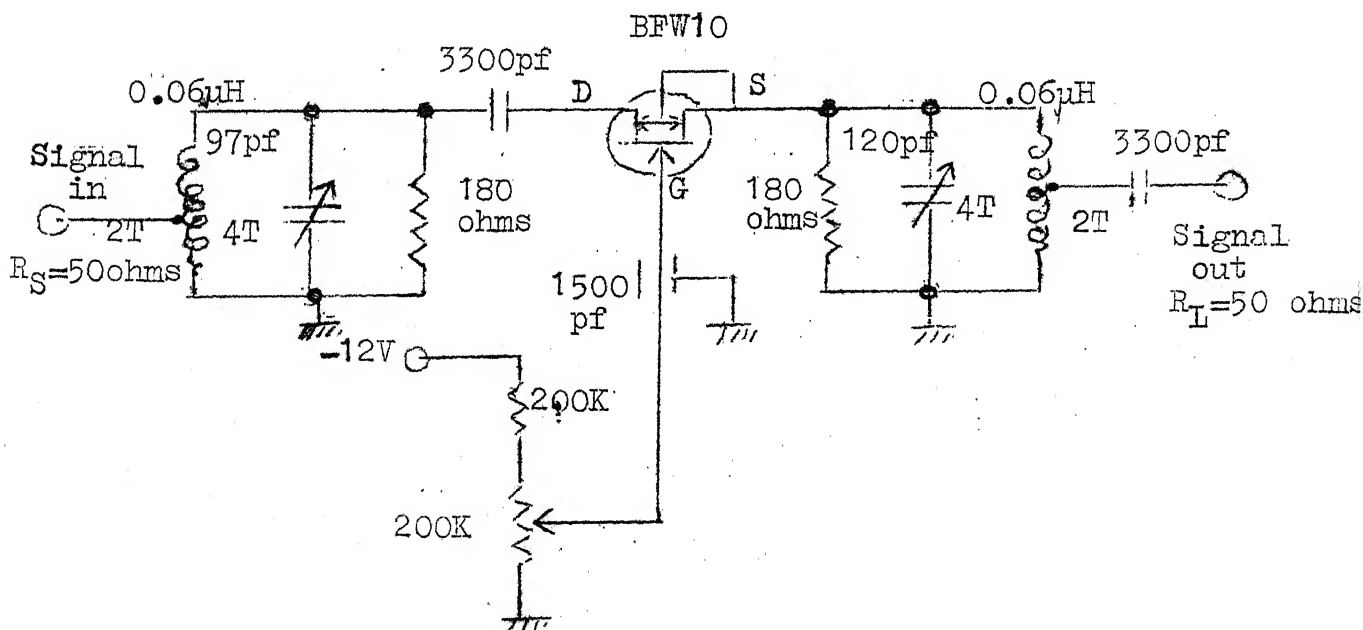
$$C_2 = 115 - (C_{stray} + C_{gs} + C_{ds} (\mu + 1)) \text{ pf}$$

Experimentally,  $C_2$  is determined and found to be 120 pf.

### 3.1.7.3 Circuit Diagram:

Signal Attenuator circuit diagram with component values is given in Fig.3.7.

Fig.3.7: Circuit Diagram of Signal Attenuator



### 3.1.8 CONSTRUCTION:

3.1.8.1 As with most high frequency circuits, careful mechanical layout is necessary to minimize the coupling between the input and output stages. The components with very short leads have been used to minimize stray inductance. The input and output tank circuits have been shielded effectively from the device and the biasing circuit and the signal attenuator block itself has been in turn shielded from the rest of the circuitry. Component wiring has been printed on an epoxy glass printed board to minimize the signal losses.

3.1.8.2 Signal level control facility has been provided. Signal level can be monitored by adjusting  $R_4$  by means of which the negative voltage applied to the gate of the device varies which in turn alters the degree of attenuation of the signal.

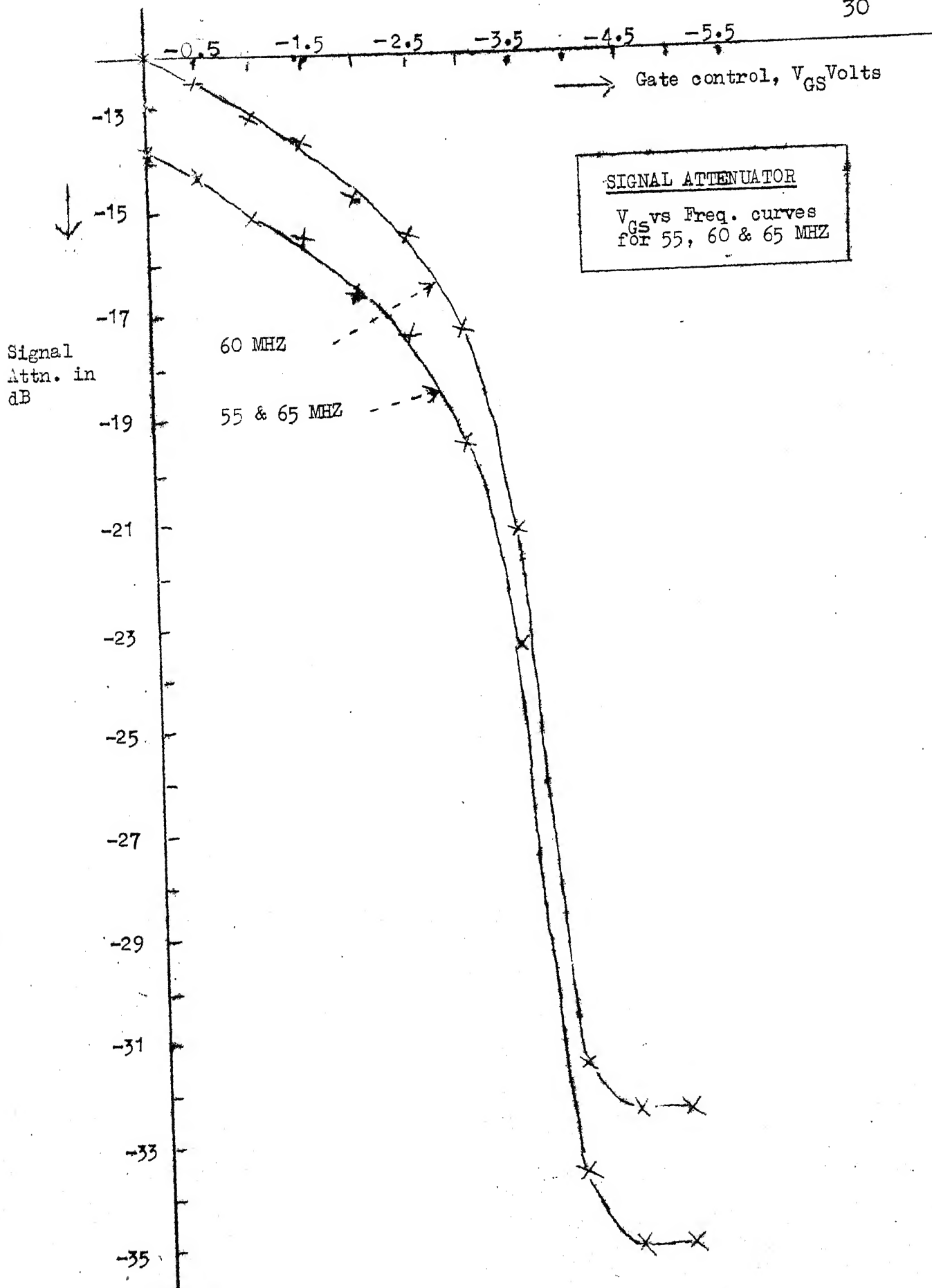
### 3.1.9 PERFORMANCE:

The circuit performance is measured at different frequencies for different gate voltages. The results are given in Table 3.1 and the circuit response in the curve. This performance is shown as a function of  $-V_{GS}$ , negative voltage applied to the gate of the device for different frequencies.

Table: 3.1      EXPERIMENTAL OBSERVATIONS

Level of Input signal to the attenuator = 320 mV (unloaded)  
160 mV (loaded)

Gate control Voltage, $V_{GS}$ in Volts	Output of Attenuator in millivolts at				Signal Attenuation in dB at			
	55 MHz	60 MHz	65 MHz	55 MHz	60 MHz	65 MHz	55 MHz	60 MHz
0	32.5	40	32.5	-13.8	-12	-13.8	-13.8	-13.8
-0.5	31	38	31	-14.3	-12.5	-14.3	-14.3	-14.3
-1.0	28	35	28.5	-15.1	-13.2	-15	-15	-15
-1.5	27	33	27	-15.5	-13.7	-15.5	-15.5	-15.5
-2.0	23.5	29.3	23.5	-16.6	-14.7	-16.6	-16.6	-16.6
-2.5	21.5	27	21.5	-17.4	-15.5	-17.4	-17.4	-17.4
-3.0	17	21.8	17.3	-19.5	-17.3	-19.3	-19.3	-19.3
-3.5	10.8	14	11	-23.4	-21.2	-23.3	-23.3	-23.3
-4.0	3.3	4.2	3.3	-33.7	-31.6	-33.7	-33.7	-33.7
-4.5	2.8	3.8	2.8	-35.1	-32.5	-35.1	-35.1	-35.1
-5.0	2.8	3.8	2.8	-35.1	-32.5	-35.1	-35.1	-35.1



## 3.2 NOISE GENERATOR<sup>3,4</sup>

### 3.2.1 INTRODUCTION:

Commercial noise sources have used thyatron kept in transverse magnetic field as the basic source of noise current. In the present system, however, a reverse biased p-n junction is used.

### 3.2.2 DESIGN SPECIFICATIONS:

The noise source is intended to meet the following specifications:

3.2.2.1 Output Spectrum: 3dB points, 51 and 69 MHz

3.2.2.2 Output level : Variable from 2 mV to 10 mV p-p

3.2.2.3 Output impedance: 50 ohms

### 3.2.3 NOISE GENERATION TECHNIQUE<sup>3</sup>

In the case of reverse biased p-n junction, reverse current,  $I$  may be expressed as

$$I = MI_0$$

where  $I_0$  is the theoretical reverse current

and  $M$  is the multiplication factor given by

$$M = \frac{1}{1 - \left(\frac{V_a}{V_{br}}\right)^m}$$

where  $V_a$  is the applied voltage,

$V_{br}$  is the breakdown voltage

and  $m \approx 3$  for silicon and n-type germanium

The reverse breakdown voltage,  $V_{br}$  is a function of doping levels. If  $V_{br} > 7V$ , the diode is said to breakdown in avalanche mode. In the transition region, the high current discharges are called as microplasma. It is found that this gives rise to random noise current in the device. These avalanche breakdown microplasmas occur preferentially where dislocations pass through the junction.

### 3.2.4 CIRCUIT CONFIGURATION<sup>4</sup>:

#### 3.2.4.1 Noise Generator:

Fig.3.8 shows a simple arrangement which exploits the above phenomena.  $R_2$  is used to vary the reverse current,  $I_R$  to bias the zener diode near the knee and the noise voltage is developed across  $R_3$ .

Microplasma - noise generation takes place only in a certain range of diode currents,  $I_1 < I < I_2$  where  $I_1$  and  $I_2$  depend upon the surface properties of device and vary from unit to unit. The output amplitude of the noise varies if the bias changes in the above range.

The amplitude probability distribution of stationary Gaussian noise current is described by

$$P(X) = \frac{1}{\sqrt{2\pi} \sigma} \exp \left( -\frac{(X-m)^2}{2\sigma^2} \right)$$

where

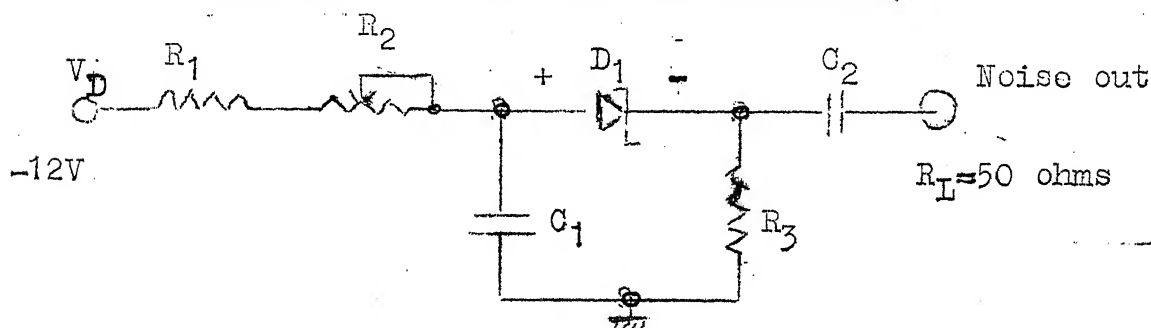
$\sigma$  = rms value of the current

$m$  = mean value of the current

$X$  = random noise current

From this, it can be deduced that the instantaneous noise voltage lies within  $\pm 3\sigma$  for 99.7 percent of time. Thus an amplifier used to provide noise output of  $\sigma$  volts rms must be able to handle the instantaneous peaks of  $\pm 3\sigma$  volts if significant errors due to overloading are to be avoided.

Fig.3.8: Wide band noise source:



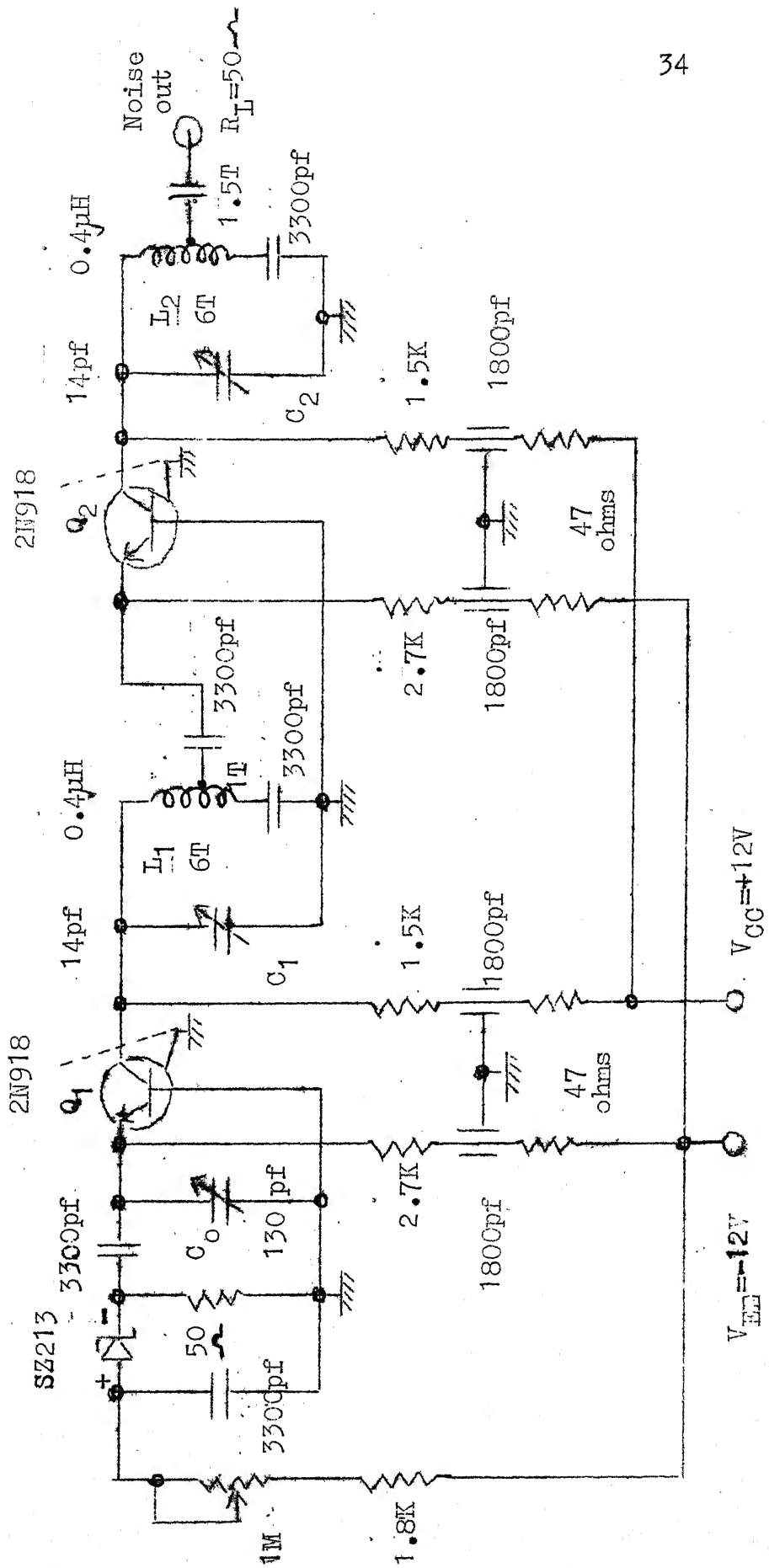
#### 3.2.4.2 Biasing:

The device chosen is SZ213 the reverse breakdown voltage,  $V_{br}$  of which is about 8.2 volts. At the transition region where microplasma phenomena occurs, the reverse current is found to be about 30 to 40  $\mu$ a.  $R_2$  is adjusted to achieve this.  $R_1$  is chosen so as to draw a maximum reverse current of 2ma when  $R_2 = 0$ .

#### 3.2.4.3 Noise Amplifier:

A two-stage common-base tuned amplifier has been used to boost the noise output developed across  $R_3$  to get the

Fig.3.9: CIRCUIT DIAGRAM OF NOISE GENERATOR AND AMPLIFIER



required noise level with specified noise output spectrum. The tank circuits of the two stages of the amplifier are stagger-tuned to get the required bandwidth. The stages are identical to those in IF amplifier block described later. The complete circuit diagram of noise generator and amplifier block is shown in Fig.3.9.

### 3.3 LINEAR ADDITION OF SIGNAL AND NOISE<sup>5</sup>.

#### 3.3.1 INTRODUCTION:

Linear addition is the process of combining two or more signals from different sources into one composite signal. Basic characteristics of linear addition are given below.

- (a) Signals from one source should not appear at any of the other sources i.e., there must be good isolation between the output and input sections of the circuitry.
- (b) No additional frequencies or distortion should be added by the circuitry.

#### 3.3.2 COMMON-EMITTER TO COMMON-BASE CASCODE CIRCUIT:

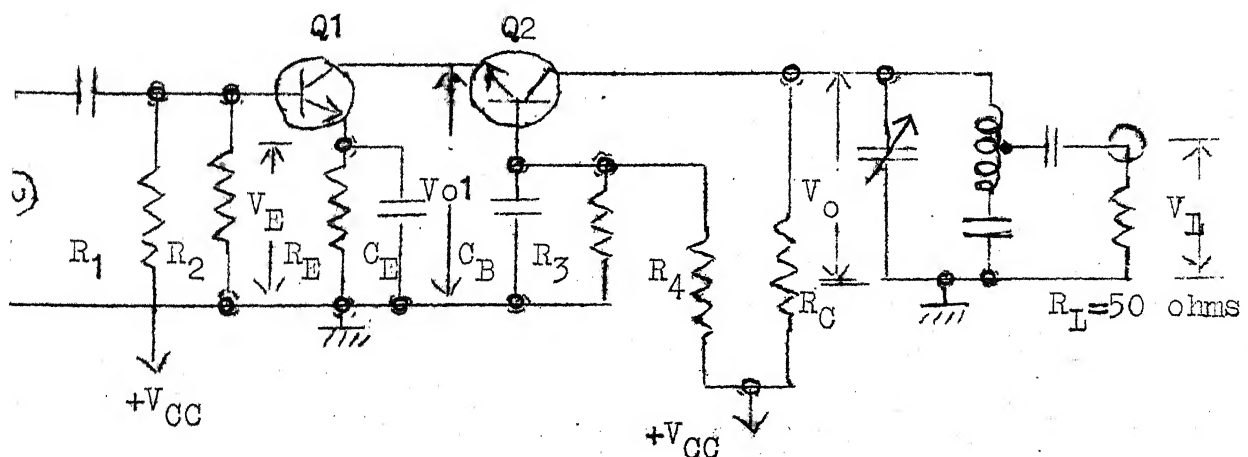
The circuit diagram using IC3028A with common-emitter to common-base cascode arrangement is shown in Fig.3.10. The two advantages obtained from the cascode arrangement of CE to CB stages are given below.

- (a) There is a minimum of internal feedback from the output to the input terminal. Voltage swings at

the collector of  $Q_2$  will couple the energy back through  $C_{bc2}$  to its base and be bypassed through  $C_B$  to the ground. Voltage swings at the collector of  $Q_1$  are developed across the low-input resistance of  $Q_2$ . The  $g_m R_L$  multiplier for  $C_{bc1}$  will be low and superior high frequency performance can be expected. This reduced internal feedback makes it possible to have a tuned circuit for a load without incurring oscillations.

- (b) The output voltage swing can be large. When both transistors  $Q_1$  and  $Q_2$  are near saturation,  $V_O$  approaches the voltage across  $C_E$  or  $V_E$ . When both  $Q_1$  and  $Q_2$  are near cut-off,  $V_O$  approaches  $V_{CC}$ . Therefore, the total peak-to-peak output voltage swing is nearly  $(V_{CC} - V_E)$ .

Fig.3.10: Common-emitter to Common-base cascode circuit



### .3 CIRCUIT CONFIGURATION:

The schematic diagram for linear addition of the incoming signal and the locally generated noise is shown in Fig.3.12. IC type CA3028A has been employed for CE to CB cascode arrangement. Manufacturer's specifications of CA3028A have been given in Appendix-A. Two cascode circuits are used one for each of the two signals to be added and the addition process is carried out by mixing the signal currents from both  $Q_2$  and  $Q_2'$  in coupling resistor,  $R_C$  shunted by the output tank circuit and the input resistance of IF amplifier stage. The inductance coil of the tuned circuit is tapped down to feed  $R_L$  of 30 ohms load which is the input resistance of the following IF amplifier stage.

In the schematic diagram, the digits 2 to 6 refer to the terminal numbers of CA3028A.  $S_1$  indicates the incoming signal,  $S_2$  the locally generated noise and  $R_L$  the input resistance of the following IF stage.

The collectors of  $Q_2$  and  $Q_2'$  offer good isolation between the two channels (i.e., signal and noise). The fact that the output impedances  $R_{O1}$  and  $R_{O2}$  at the collector terminals of  $Q_2$  and  $Q_2'$  (CB configuration) are very high when compared to the effective load,  $R_C' = \frac{R_C}{2} = 75$  ohms ensures excellent isolation between the two channels.

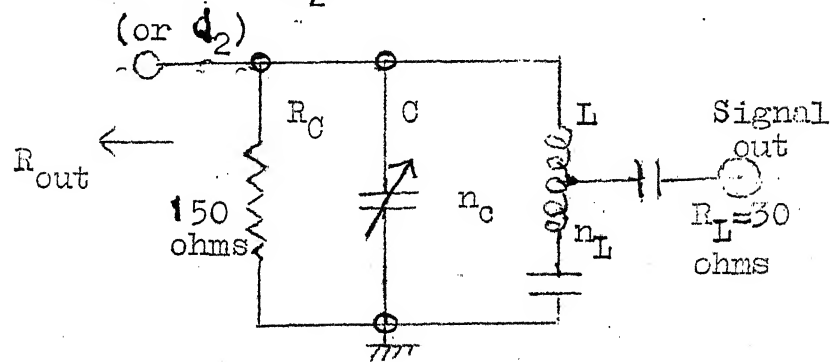
### .3.4 CIRCUIT DESIGN:

#### .3.4.1 Biasing:

$I_{C1}$  and  $I_{C2}$  are the collector currents of  $Q_2$  and  $Q_2'$  of the two cascode circuits. The biasing resistors are chosen so as to make each of them equal to 5 ma. Total current,  $I_C$  flowing through common collector resistor of 150 ohms will be 10 ma. The dc voltages appearing at the terminals of CA3028A are shown in Fig.3.12.

#### .3.4.2 Output network: Collector of $Q_2$

Fig.3.11



$R_{out}$  in cascode arrangement is very high when compared to  $R_C$  of 150 ohms. Therefore, the resistance shunting  $L$  is 150 ohms.

Centre frequency,  $f_o = 60 \text{ MHz}$

Band width chosen,  $B = 20 \text{ MHz}$

Therefore,  $Q_L = \frac{f_o}{B} = 3$

Using equations 3.1 to 3.5,

$L = 0.066 \mu\text{h}$  ( $d=0.35''$ ,  $l=0.6''$ ,  $n_c=4$  turns)

$C = 105 \text{ pf}$

$n_L = 1.75$  turns from ground.

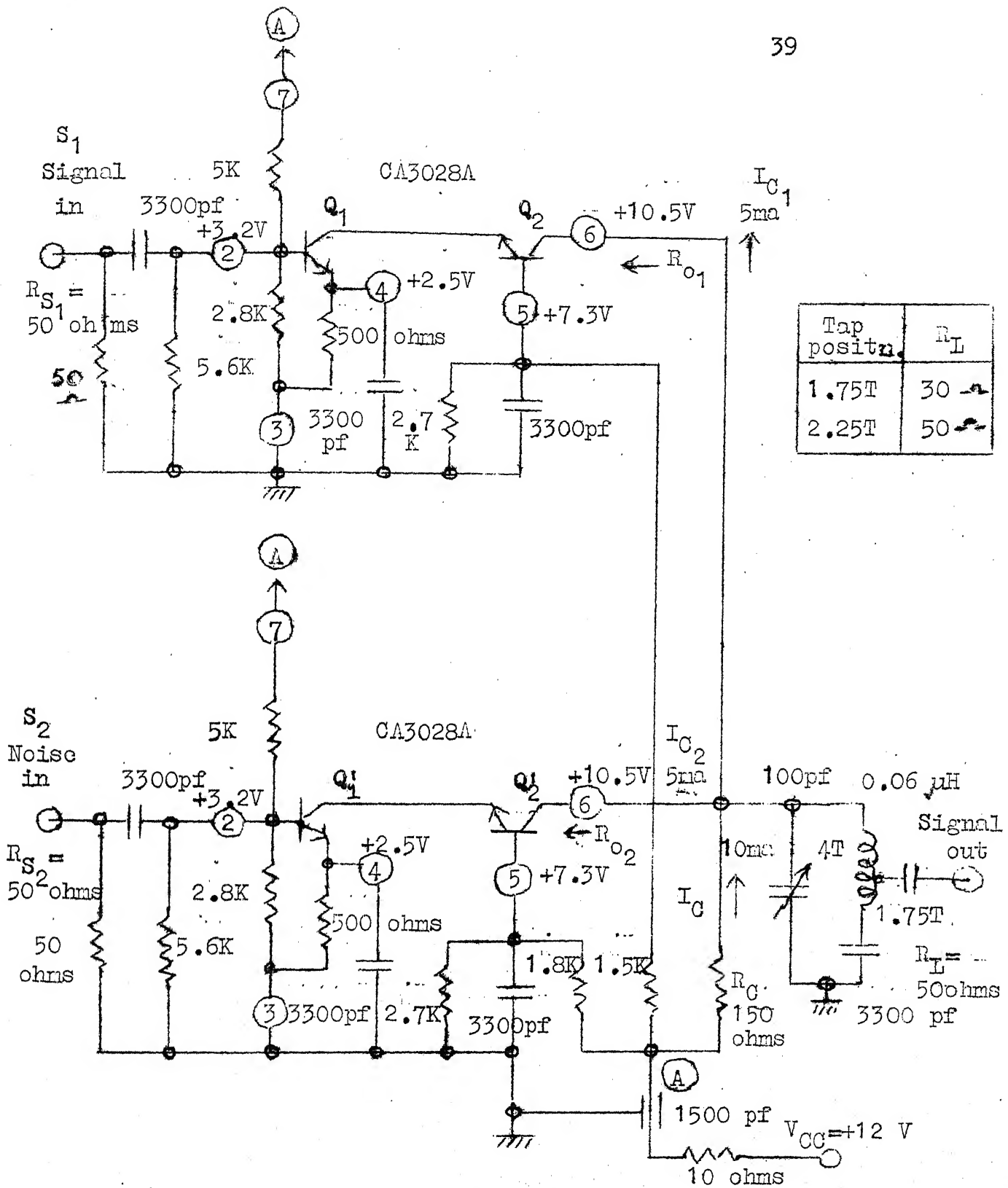


FIG.3.12: CIRCUIT DIAGRAM OF LINEAR ADDITION OF SIGNAL AND NOISE

### 3.4 IF AMPLIFIER<sup>7,8,9</sup>

#### 3.4.1 INTRODUCTION:

Narrow band amplifiers are characterized by frequency discrimination and provide large gain over a specified bandwidth. Such amplifiers are generally tuned amplifiers using resonant circuits to obtain desired selectivity and centre frequency.

#### 3.4.2 DESIGN METHODS:

In IF amplifiers, the internal feedback of the device causes the transistor input impedance to be a function of load impedance which makes the multistage IF amplifier alignment difficult. Design methods to overcome the internal feedback effects are

- (a) Neutralization method and
- (b) Mismatching method

Neutralization method is to neutralize the effect of the reverse feedback ratio or unilateralize the transistors in the amplifier. This technique is usually limited to a narrow-band, high gain applications.

Mismatching method involves mismatching the device at its input and output terminals. The advantages of this method are given below.

- (a) Stability for all devices of particular type.
- (b) Useful stable gains upto very high frequencies
- (c) Easy practical multistage amplifier alignment.

Mismatching technique has been chosen for IF and Noise amplifier stages as it suits the requirements of stable gain at high frequencies and over wideband.

### 3.4.3 DESIGN SPECIFICATIONS:

- 3.4.3.1 Centre frequency,  $f_o$  = 60 MHZ
- 3.4.3.2 Overall Band-width, B = 10 MHZ
- 3.4.3.3 Voltage gain,  $V_G$  = 35 dB
- 3.4.3.4 Input and output impedances = 50 ohms each
- 3.4.3.5 Design method = Mismatching technique

### 3.4.4 CIRCUIT DESIGN:

- 3.4.4.1 The device chosen is 2N918, silicon, NPN type, Fairchild transistor. The manufacturer's specifications for 2N918 are given in Appendix A.

For common-base configuration at  $I_C = 4\text{ma}$ ,  $V_{CE} = 6\text{ V}$  and  $f_o = 60\text{ MHZ}$ , the input and output impedances are as given below:

- Input resistance,  $R_{ib}$  = 30 ohms
- Input inductance,  $L_{ib}$  =  $0.05\mu\text{h}$
- Output resistance,  $R_{ob}$  = 2.5 K ohms
- Output capacitance,  $C_{ob}$  = 4 pf

The circuit diagram is given in Fig.3.13. Three stages of common-base mode have been used.

#### 3.4.4.2 Bandwidth per stage:

Overall half power bandwidth for  $n$  identical stages in terms of the single stage band-width is given by the expression

$$B = B_S (2^{1/n} - 1)^{1/2} \approx \frac{B_S}{1.2n} \quad (3.6)$$

where  $B$  is the overall bandwidth of  $n$  cascaded stages,  
 $B_S$  is the band-width of individual, identical stages,  
 $n$  is the number of stages.

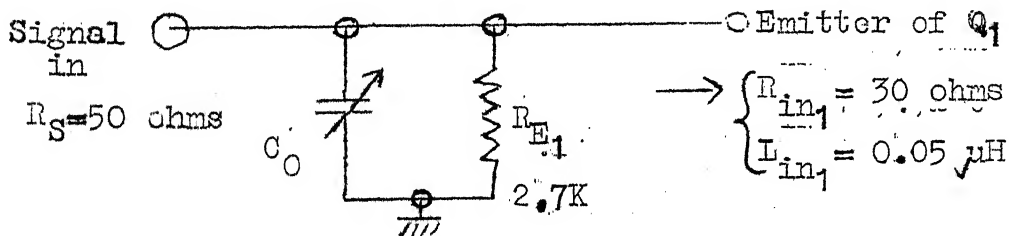
For 3-stage IF amplifier,  $n=3$  and  $B = 0.5B_S$

For  $B = 10 \text{ MHz}$ ,  $B_S = 20 \text{ MHz}$

$\therefore$  Bandwidth per stage = 20 MHz

Loaded  $Q$  of each tank circuit,  $Q_L = \frac{f_o}{B_S} = \frac{60}{20} = 3$

#### 3.4.4.3 Input network of the 1st stage:



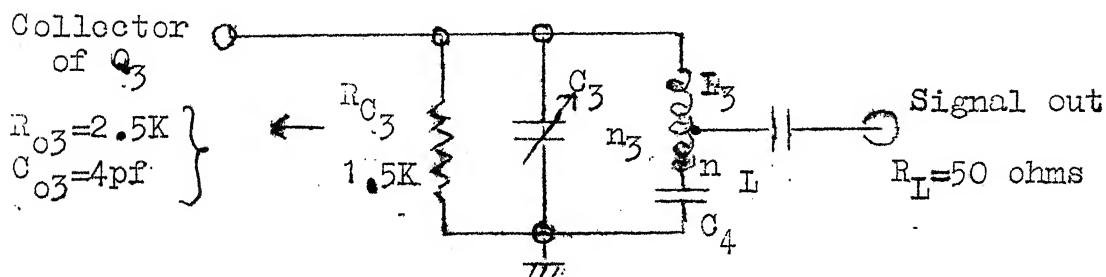
It is decided to resonate  $L_{in1}$  with  $C_0$  at 60 MHz and allow slight mismatch between  $R_S$  and  $R_{in1}$  which improves the stability of the amplifier. In any case, the amount of mismatch can be reduced or controlled by proper adjustment of the tap on the output tank circuit of the preceding stage (i.e., Linear

addition of signal and noise) from which the signal is fed to the input network of the 1st stage of IF amplifier.

$$C_o = \frac{1}{W_o^2 L_{in_1}} = \frac{2.645^2 \times 10^{-18}}{0.05 \times 10^{-6}} = 140 \text{ pf}$$

Allowing for stray and wiring capacitances,  $C_o = 130 \text{ pf}$ .

#### 3.4.4.4 Output network of last (3rd) stage:



Resistance shunting  $L_3 = R_{O3} \parallel R_{C3} = 2.5 \text{ K} \parallel 1.5 \text{ K} = 940 \text{ ohms}$

From equations 3.1 to 3.5, we get for  $Q_L=3$ ,

$$L_3 = 0.4 \mu\text{h} \quad (l=0.4'' ; d = 0.55'' ; n_3 = 6 \text{ turns})$$

$$\text{Total capacitance across } L_3, C = 18 \text{ pf} = C_{O3} + C_3$$

$$\text{Therefore, } C_3 = 14 \text{ pf}$$

$$n_L = 1.5 \text{ turns from ground (for } R_L=50 \text{ ohms)}$$

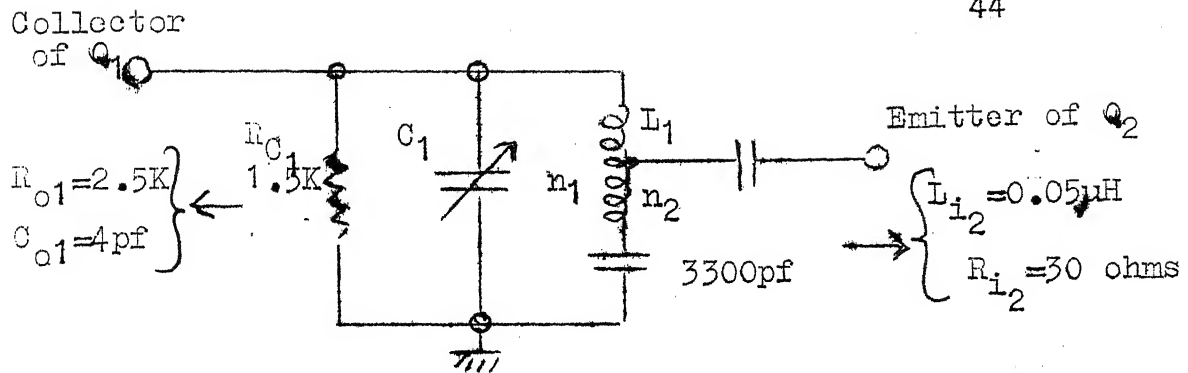
$$= 1 \text{ turn from ground (for } R_L = 30 \text{ ohms)}$$

$L_3$  and  $C_4$  resonate at a frequency nearly 5 times lower than 60 MHz. Choosing resonant frequency of 5 MHz,

$$C_4 = 0.0033 \mu\text{-F}$$

#### 3.4.4.5 Interstage coupling network:

Proceeding on the same lines as given under clause



3.4.4.5, the chosen value of  $L_1 = 0.4 \mu\text{h}$ .  $L_{i2} = 0.05 \mu\text{h}$  is reflected as  $2 \mu\text{h}$  onto the left hand side of  $L_1$  and the effect of it has been neglected in the calculations.

$$C_1 = 14 \text{ pf},$$

$$n_1 = 6 \text{ turns, and}$$

$$n_2 = 1 \text{ turn from ground}$$

#### 3.4.4.5 Mid-band voltage gain:

Overall mid-band voltage gain of 3-stage Amplifier is

$$\frac{V_L}{E_S} = \left( \frac{\beta_o}{\beta_o + 1} \right)^3 \frac{R_o \sqrt{R_o R_L}}{R_i (R_S + R_i)} = 73.3 = (37 \text{ dB})$$

where  $R_o$  is the output resistance of CB stage,  
 $R_i$  is the input resistance of CB stage,  
 $R_S$  is the source resistance and  
 $R_L$  is the load resistance.

#### 3.4.5 CONSTRUCTION:

Careful mechanical layout has been carried out to minimize parasitic inductance and capacitance. Transistor sockets can be used even at these frequencies because small capacitances are not as important as low lead-inductance.

Component leads are cut as short as possible to minimize stray inductance. The output network of each stage is shielded well from its input network. The output of IF amplifier is available through an IF connector, type UG 291/U which is fixed to the box.

#### 3.4.6 PERFORMANCE:

The experimental observations of the IF amplifier are given in Table 3.2 and the performance is shown as a function of frequency in the response curve. These gain measurements were based with

- (a) a 50 ohm source and a 50 ohm load and
- (b) the three stages stagger-tuned to get an overall band-width of 15 MHZ.

Fig.3.13: CIRCUIT DIAGRAM OF IF AMPLIFIER

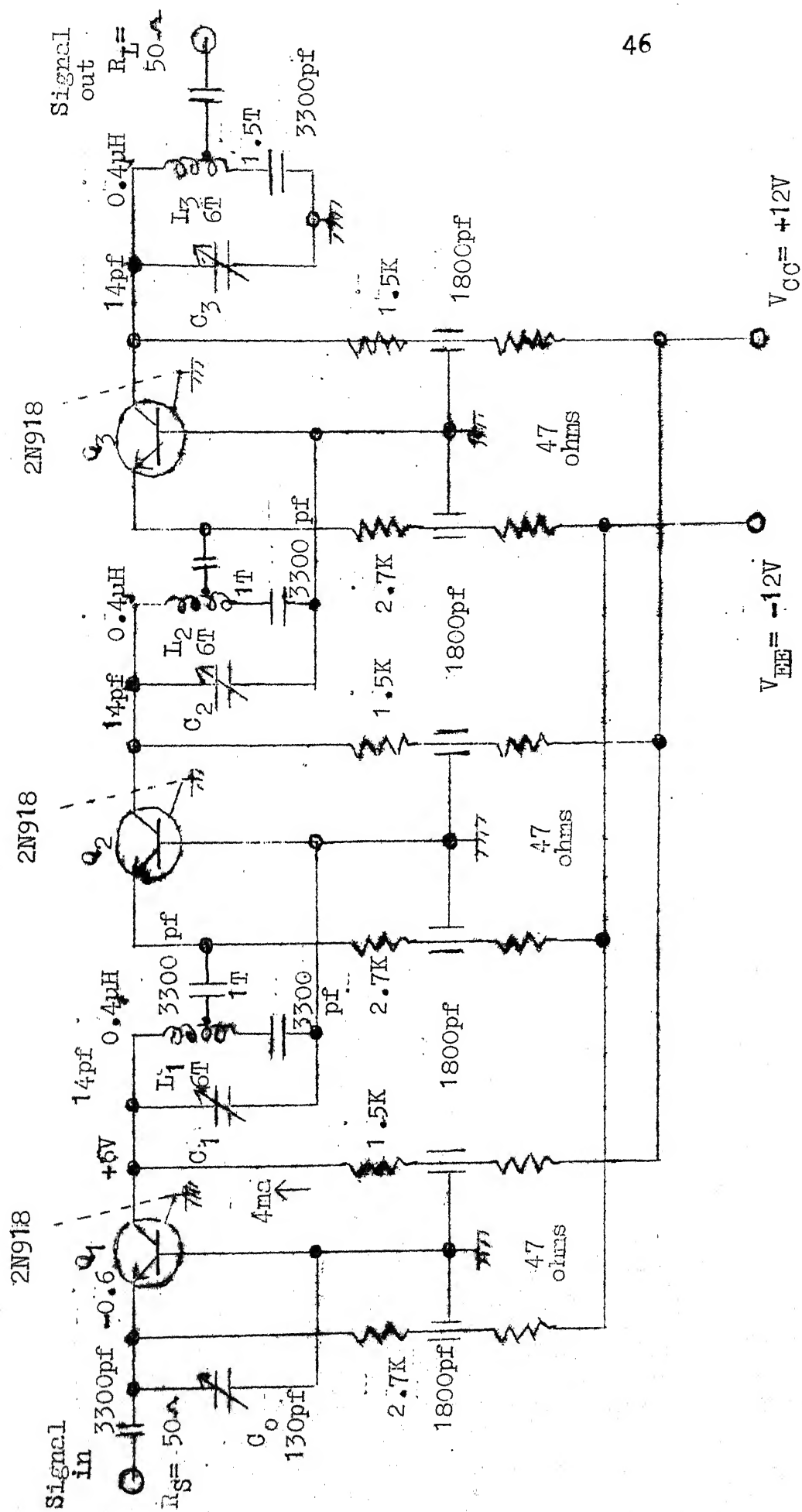


TABLE: 3.2      EXPERIMENTAL OBSERVATIONS

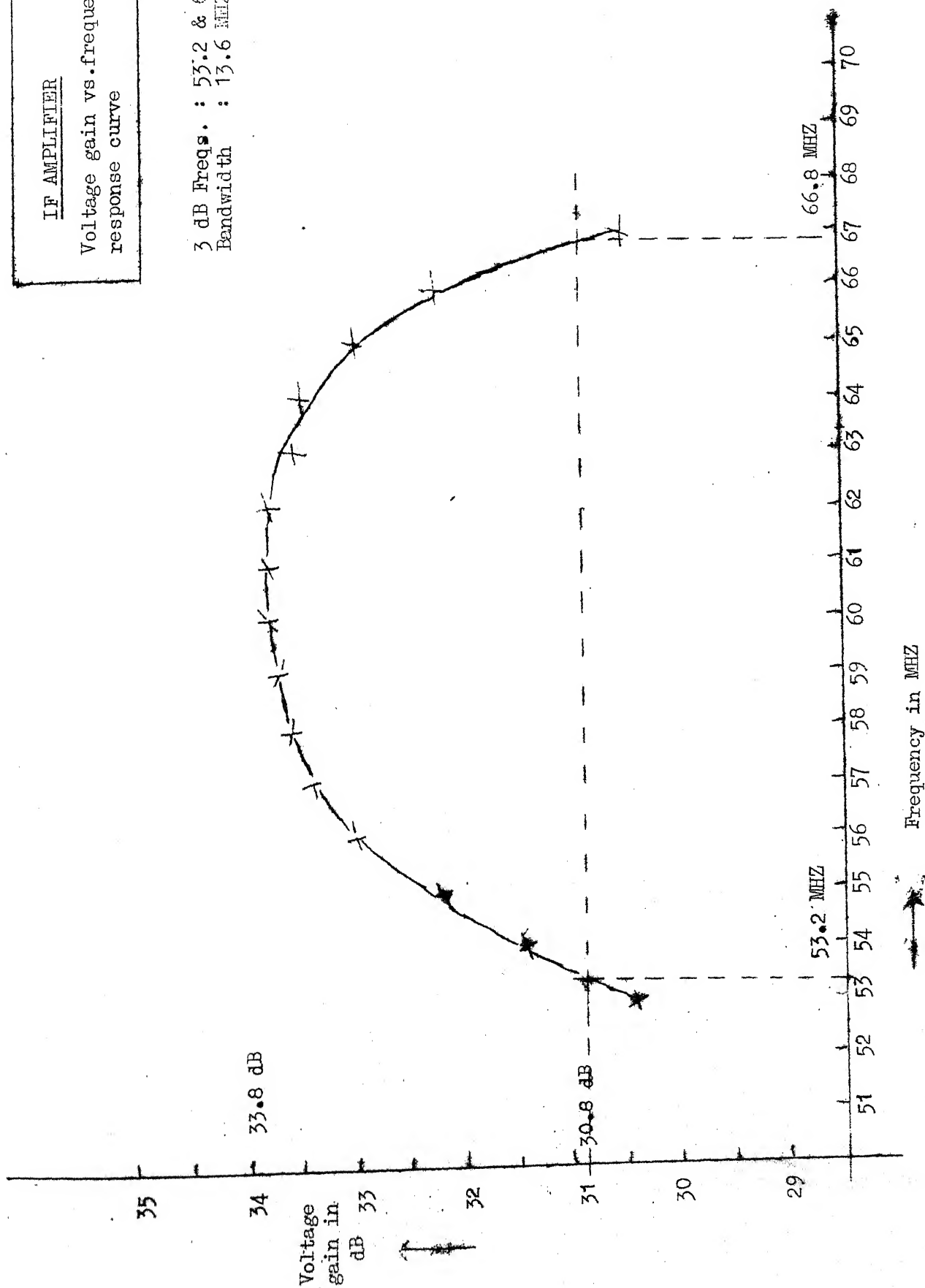
Level of Input signal to IF Amplifier,  $A_i = \begin{cases} 3.25 \text{ mV p-p (unloaded)} \\ 1.62 \text{ mV p-p (loaded)} \end{cases}$

Input signal frequency in MHz	IF Amplifier output, $A_v$ in mV	Voltage gain	
		$A_v/A_i$	$20 \log_{10} A_v/A_i$ dB
67	55	33.8	30.5
66	68	42	32.4
65	73	45	33
64	76.5	47	33.5
63	77.6	47.8	33.6
62	79.5	48.9	33.8
61	80	49.2	33.8
60	80	49.2	33.8
59	79.3	48.8	33.7
58	77.5	47.8	33.6
57	76	46.7	33.4
56	71.5	44.4	33
55	66	40.6	32.2
54	60	37	31.3
53	54	33.2	30.4

IF AMPLIFIER

Voltage gain vs. frequency  
response curve

3 dB Freqs. : 53.2 & 66.8 MHz  
Bandwidth : 13.6 MHz



### 3.5 MULTIPLIER<sup>13,5</sup>

#### 3.5.1 INTRODUCTION:

In this section, a single differential pair employed as a multiplier for normal and quadratic channels has been discussed. The incoming modulated signal ( $S_1$ ) forms one of the inputs to both multipliers while the other input ( $S_2$ ) is the local 60 MHz IF which is in phase with the transmitted IF for normal channel and  $90^\circ$  out of phase for quadratic case. To avoid any interaction between the multipliers, there must be good isolation between input and output sections of each multiplier.

#### 3.5.2 CIRCUIT ANALYSIS:

3.5.2.1 The differential pair multiplier configuration is shown in Fig. 3.14. The circuit gives good isolation between the output and input sections.

For  $S_1$ ,  $Q_1$ - $Q_2$  combination acts as CC to CB cascode arrangement and there is no phase shift between  $S_1$  and  $V_o$ . External resistor at collector of  $Q_1$  is omitted so that no signal voltage can be developed at collector of  $Q_1$  for coupling back through  $C_{bc1}$  to the base of  $Q_1$ . Also, the base of  $Q_2$  is shunted with suitable capacitor,  $C_B$  so that any signal voltage fed back from collector of  $Q_2$  through  $C_{bc2}$  will be bypassed to ground. Consequently, the circuit has good high-frequency performance.

For  $S_2$ ,  $Q_3$ - $Q_2$  combination acts as CE to CB cascode arrangement and there is phase reversal between  $S_2$  and  $V_O$ . Voltage swings at collector of  $Q_2$  will couple the energy back through  $C_{bc2}$  to its base and be bypassed to ground through  $C_B$ . Also, voltage swings at collector of  $Q_3$  are developed across low-input resistance of  $Q_2$ . The low gain and the consequent smaller Miller capacitance of  $Q_3$  ensure improved high-frequency performance.

### 3.5.2.2 Multiplier Out-put:

Voltage gain of a differential amplifier is readily shown to be proportional to  $g_m$  of  $Q_2$  which because of its linear dependence on  $i_{c3}$  can be effectively controlled by  $S_2$ . Multiplier output,  $V_O$  in terms of  $S_1$  and  $S_2$  is shown<sup>5</sup> to be

$$V_O = S_1 (A_1 + A_2 S_2) \quad (3.7)$$

where 
$$A_1 = \frac{I_{c3} R_c}{0.1} = \left( \frac{V_{B3} - V_{BE3}}{R_{E3}} \right) \frac{R_c}{0.1}$$

and 
$$A_2 = R_c / 0.1 \left( R_{E3} + \frac{r_{i3} + R_B}{\beta_{Q3} + 1} \right)$$

Let  $S_1(t)$  be the PS keyed signal and  $S_2(t)$ , the local IF in phase with transmitted IF.

$$S_1(t) = f(t) \cos \omega_c t \quad \text{and} \quad S_2(t) = \cos \omega_c t \quad \text{where} \quad f(t) = \pm 1$$

$$V_O(t) = K_1 f(t) \cos^2 \omega_c t + K_2 f(t) \cos \omega_c t \quad (3.8)$$

$$= \frac{k_1}{2} f(t) + \frac{k_1}{2} f(t) \cos 2\omega_c t + k_2 f(t) \cos \omega_c t$$

where  $k_1$  and  $k_2$  are constants. If  $f(t) \longleftrightarrow F(W)$ ,

$$V_0(W) = \frac{k_1}{2} F(W) + \frac{k_1}{4} (F(W+2W_c) + F(W-2W_c)) \\ + \frac{k_2}{2} (F(W+W_c) + F(W-W_c))$$

The original signal  $f(t)$  can be recovered by using a low-pass filter which will allow  $F(W)$  to pass and will attenuate the remaining components centred around  $\pm 2W_c$  and  $\pm W_c$ .

### 3.5.3 CIRCUIT DESIGN:

#### 3.5.3.1 Low pass filter:

The  $R_c - C_c$  combination in the collector of  $Q_2$  forms the low-pass filter. Taking into consideration the effect of  $R_L = 50$  ohms, total resistance shunting  $C_c$  is  $R_c \parallel R_L = 25$  ohms. Choosing cut-off frequency,  $f_c$  of 12 MHz,

$$C_c = (1/2\pi f_c)(R_c \parallel R_L) = 500 \text{ pf.}$$

#### 3.5.3.2 Phase-shifting of Network<sup>16</sup>:

A  $\pi$ -network which introduces a phase lag of  $90^\circ$  is designed to operate at 60 MHz frequency for input and output impedances of 50 ohms each and the circuit diagram is shown in Fig. 3.15.

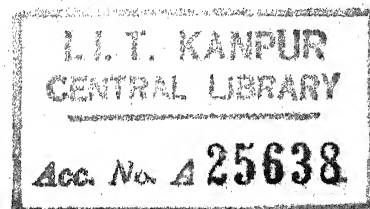


Fig.3.14 : SCHEMATIC DIAGRAM OF MULTIPLIER

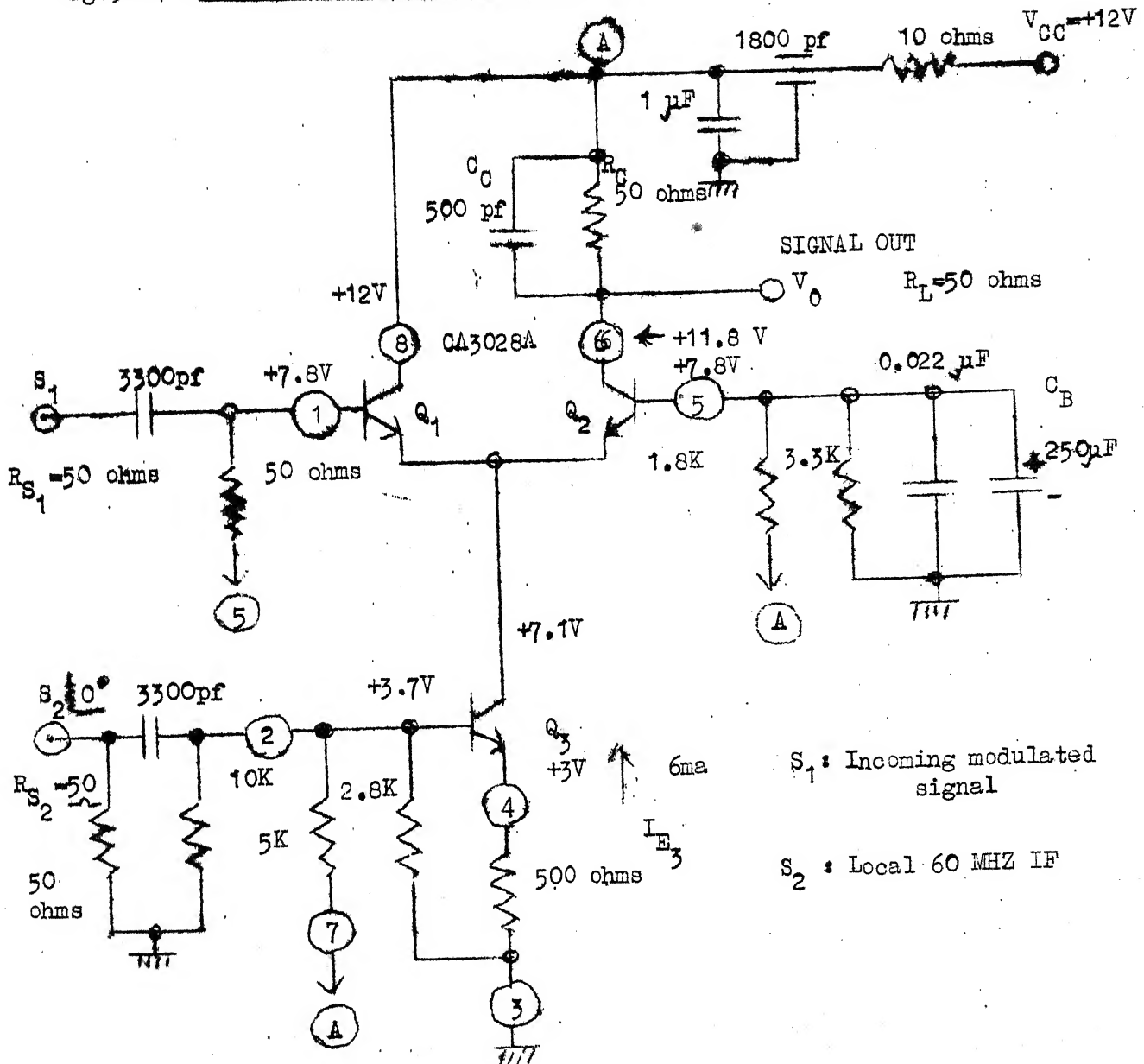
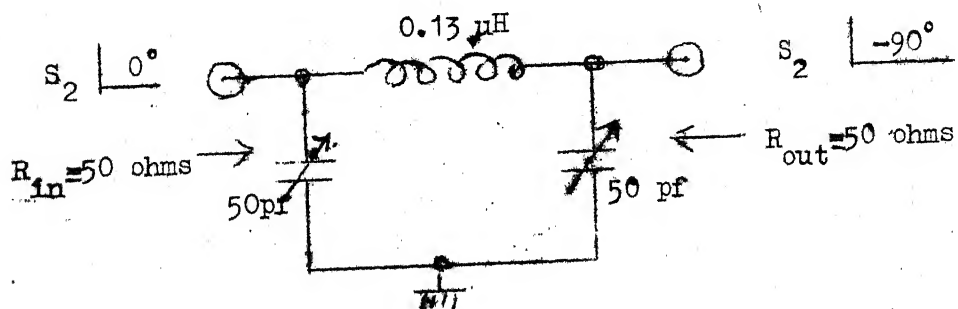


Fig.3.15 : 90° PHASE SHIFTING NETWORK



### 3.6 VIDEO AMPLIFIER 7,8,14

#### 3.6.1 INTRODUCTION:

A stable video amplifier of 10 MHz bandwidth is constructed using shunt-feedback network around each stage. The use of collector-to-base feedback is a method of improving bandwidth which results in reduced (a) input and output impedances and (b) overall gain at low frequencies, trading gain for bandwidth.

#### 3.6.2 DESIGN SPECIFICATIONS:

3.6.2.1	Overall voltage gain, $A_V$	: 35 dB
3.6.2.2	Bandwidth	: 10 MHz
3.6.2.3	Input impedance	: 50 ohms
3.6.2.4	Output impedance	: 50 ohms

#### 3.6.3 DESIGN PROCEDURE:<sup>7</sup>

##### 3.6.3.1 Design Equations:

The following are the design equations for a single-stage collector feedback amplifier.

$$\text{Input resistance, } R_{in} = r_{\pi} \parallel \frac{R_F + R_L}{1 + g_m R_L} \quad (3.11)$$

$$\text{Voltage gain, } A_V = -g_m (R_L \parallel R_F) \quad (3.12)$$

$$\text{Current gain, } A_i = \frac{\beta_0 (R_L + R_F)}{r_{\pi} + R_F + (\beta_0 + 1) R_L} \quad (3.13)$$

$$\text{Shunt-feedback resistance, } R_F = \frac{A_i r_{\pi} + \beta_0 R_L (A_i - 1)}{(\beta_0 - A_i)} \quad (3.14)$$

$$\approx \frac{R_{in} r_{\pi} + R_{in} R_L (\beta_0 + 1) - R_L r_{\pi}}{r_{\pi} - R_{in}} \quad (3.15)$$

### 3.6.3.2 DC Biasing:

The Collector current in the last stage should be high enough to provide a high output voltage but the first stage collector current should be low enough to stabilize the input impedance.

### 3.6.3.3 Design of Shunt-feedback resistance:

Using equations as given under clause 3.6.3.1, the shunt feed-back resistors can be calculated starting from last stage taking into consideration the source and load impedances of 50 ohms each. The table given below gives the calculated parameters.

Amplifier stage	$I_C$ ma	$R_L$ ohms	$R_F$ ohms	$R_{in}$ ohms	$A_V$	$A_i$
3	11.4	50	280	10	20	5
2	3.8	10	200	50	1.5	8
1	1.9	50	300	50	3	4

Overall mid-band voltage gain,  $A_V = 39$ .dB

where

$R_L$  : Load/output resistance

$R_F$  : Collector feedback resistance

$R_{in}$  : ~~Source~~/Input resistance

#### 3.6.3.4 Emitter bypassing and coupling:

Electrolytic capacitors of 250  $\mu$ F in parallel with polyester type of 0.022  $\mu$ F have been used for both bypassing and coupling. The leads of capacitors are trimmed to minimum to reduce the effective series inductance.

#### 3.6.3.5 Decoupling:

With very low input and output impedances of each stage, very little signal current flows through collector resistor to be coupled back into collector supply voltage lead. Also, with each emitter bypassed to ground, very little signal current flows through the emitter resistor. Sufficient decoupling is achieved with networks shown in Fig.3.16.

### 3.6.4 CIRCUIT CONFIGURATION<sup>14</sup>

The circuit configuration of video amplifier is shown in Fig.3.16. Capacitance coupling has been employed as the amplifier may suffer from operating point stability with direct coupling. The device chosen is silicon, NPN transistor, type 2N3563 having  $f_T$  of 600 MHz and  $\beta_F$  of 20.

### 3.6.5 PERFORMANCE:

The performance of the video amplifier with resistive shunt feedback arrangement is observed with source and load impedances of 50 ohms each. The 3-dB low- and high-frequencies have been observed to be about 70 HZ and 15 MHZ respectively.

With transistors of low  $f_T$ , R-L feedback may have to be used for all the stages except the first one for good overall high frequency response and the first stage should have resistive feedback to provide a flat-input-impedance characteristic<sup>7</sup>.

## 3.7 POLARITY SENSING DETECTOR<sup>15,5</sup>

### 3.7.1 INTRODUCTION:

A symmetrical transistor amplifier followed by a difference-amplifier comparator has been used to serve as polarity sensing detector (PSD) with one of the inputs connected to ground (reference voltage) while the other measuring input to the signal. Comparator output assumes one of the two levels i.e., digital "1" or "0" for positive or negative going input signals.

### 3.7.2 CIRCUIT CONFIGURATION:

The schematic diagram of PSD is shown in Fig.3.17. The difference amplifier is highly stable because of the nature

Fig. 3.16: CIRCUIT DIAGRAM OF VIDEO AMPLIFIER

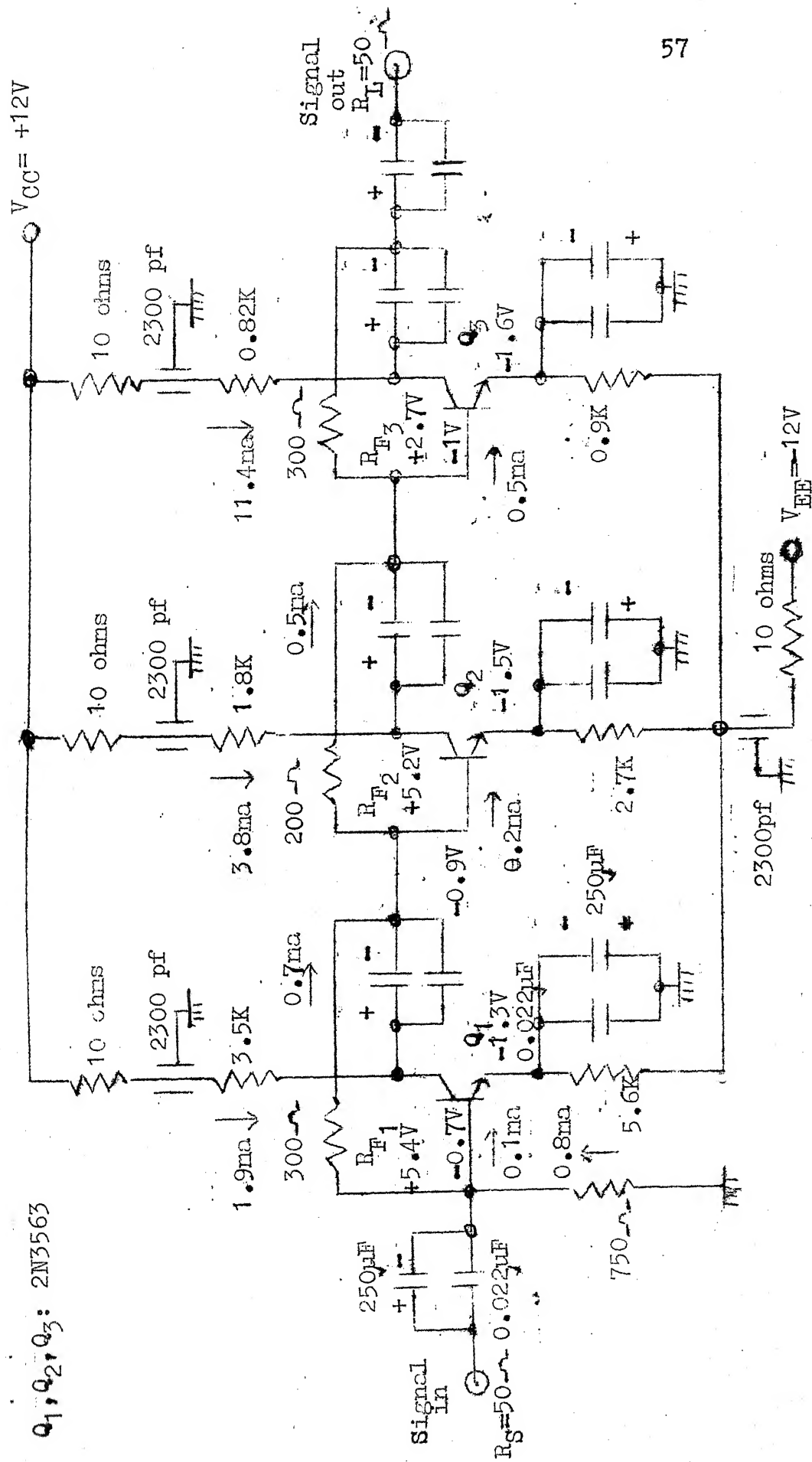


Table 3.3 EXPERIMENTAL OBSERVATIONS (Video Amplifier)

Level of Input signal,  $v_{in} = \begin{cases} 12 \text{ mV} & (\text{unloaded}) \\ 6 \text{ mV} & (\text{loaded}) \end{cases}$

Input signal freq.	Video Amp. o/p, $v_{out}$ in mV	$\frac{v_{out}}{v_{in}}$	$\frac{v_{out}}{v_{in}}$ in dB
10 MHz	320	53.3	34.5
8 "	330	55	34.8
6 "	338	56.3	35.0
4 "	344	57.3	35.2
2 "	348	58.0	35.3
1 "	350	58.3	35.3
800 KHZ	350	58.3	35.3
600 "	350	58.3	35.3
400 "	350	58.3	35.3
200 "	365	60.8	35.7
100 "	375	62.5	35.9
80 "	375	62.5	35.9
60 "	375	62.5	35.9
40 "	380	63.3	36.0
20 "	385	64.2	36.1
10 "	400	66.7	36.5
8 "	400	66.7	36.5
6 "	400	66.7	36.5
4 "	395	65.8	36.4
2 "	395	65.8	36.4
1 "	400	66.7	36.5
300 HZ	400	66.7	36.5
600 "	400	66.7	36.5
400 "	390	65.0	36.3
200 "	380	63.3	36.0
100 "	330	55.0	34.8
80 "	300	50.0	34.0
60 "	250	41.7	32.4
20 "	120	10.0	20.0

of the device, IC CA3028A used.

### 3.7.3 CIRCUIT DESCRIPTION:

When the input signal,  $v_i$  to the difference amplifier goes sufficiently positive by a few milli-volts,  $Q_3$  should turn ON to detect the crossing of zero reference in the positive direction. Conversely, when  $Q_3$  turns OFF, output goes to 0 volts to indicate that the input has crossed zero in negative direction.

#### 3.7.3.1 DC Analysis:

At balance, the input voltage,  $v_i=0$  and the dc voltages at different terminals are shown in Fig.3.17. Resistance R is adjusted so that  $Q_3$  is in active region so that the voltage at the collector of  $Q_3$  i.e.,  $v_{out} = + 2.5$  volts.

#### 3.7.3.2 $Q_3$ TURNON:

With  $v_i$  crossing zero sufficiently in positive direction such that the  $Q_{11}-Q_{12}$  develops a minimum differential output voltage that is sufficient to cut-off  $Q_{21}$  and drive  $Q_{22}$  into saturation,  $v_{O+} = V_{CC} - 7 \text{ ma} \times 0.47 \text{ K ohms} = + 1.7\text{V}$  and  $Q_3$  is driven into saturation. Thus,  $v_{out+} = + 5$  volts (digital "1").

#### 3.7.3.3 $Q_3$ TURNOFF:

With  $v_i$  crossing zero sufficiently in negative direction,  $Q_{21}$  becomes ON and  $Q_{22}$  goes into cut-off state resulting in  $v_{O-} = + 5$  volts. Thus,  $Q_3$  is OFF and  $v_{out-} = 0\text{V}$  (digital "0").

$v_i$	$Q_{21}$	$Q_{22}$	$v_0$	$Q_3$	$v_{out}$
0	Active	Active	+3.3V	Active	+ 2.5V
+ve	OFF	ON	+1.7V	ON	+ 5V (digital "1")
-ve	ON	OFF	+5V	OFF	0V (digital "0")

#### 3.7.3.4 Minimum Crossing Voltage:

(a) Considering difference-amplifier comparator circuit ( $Q_{21}$ ,  $Q_{22}$ ), total range of output swing,  $\Delta v_0$  over which the output can follow the input is

$$\Delta v_0 = I_{E_{23}} R_{C_2} = 7\text{mA} \times 0.47 \text{ k ohms} = 3.3\text{V p-p}$$

Differential voltage gain,  $A_d = \frac{\Delta v_0}{\Delta v_i} = \frac{g_m R_{C_2}}{2}$  from which the total input voltage swing required is  $\Delta v_i = 100 \text{ mv p-p}$ .

(b) Considering difference-amplifier circuit ( $Q_{11}$ ,  $Q_{12}$ ),  $\Delta v_0 = 100 \text{ mv p-p}$  and  $A_d = \frac{\Delta v_0}{\Delta v_i} = g_m R_C$  from which  $\Delta v_i = 3 \text{ mv p-p}$ .

Thus, total input voltage swing required at the input of difference amplifier to carry the output of the comparator through its entire swing of 3.3 V p-p is 3 mV p-p.

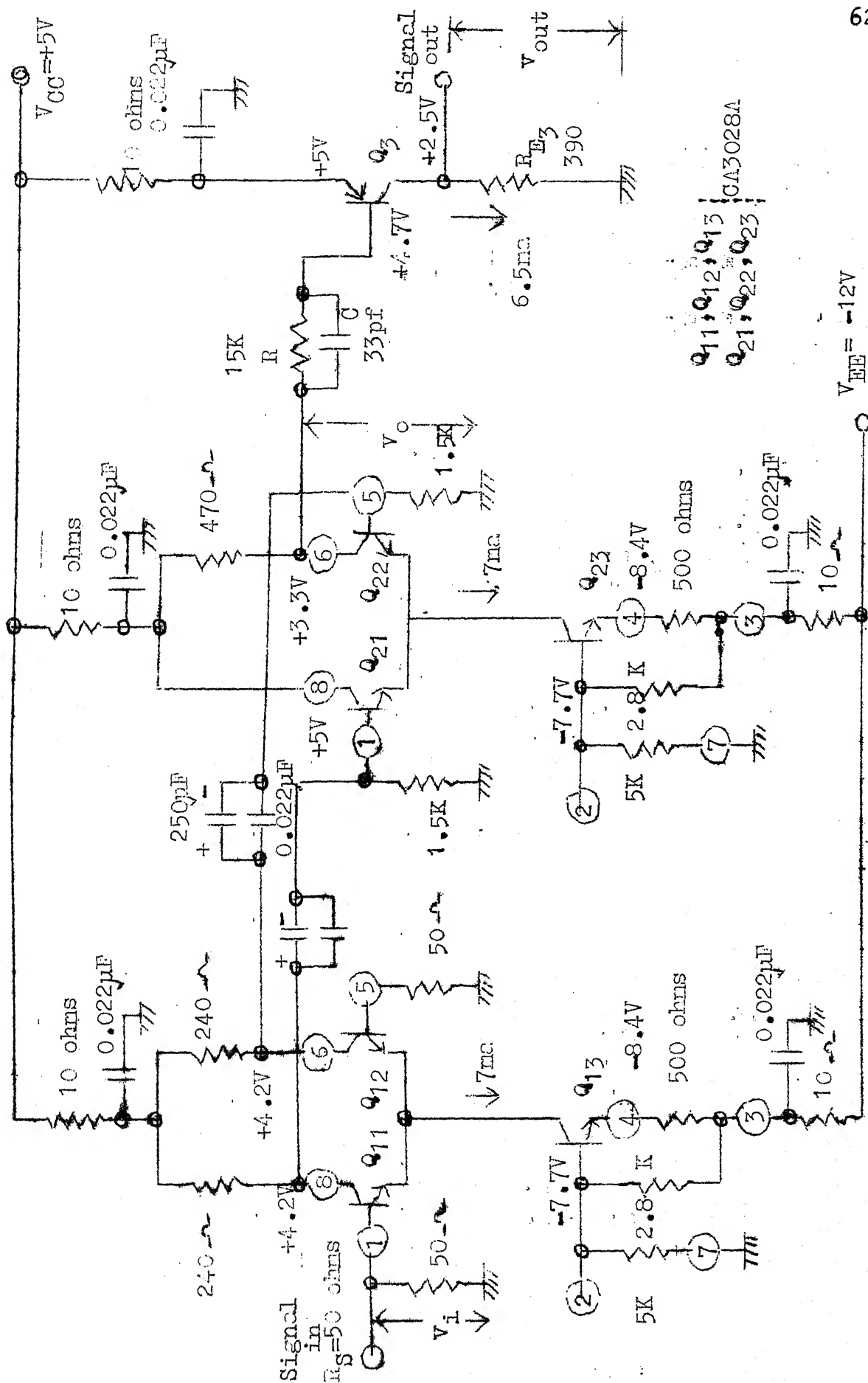
#### 3.7.4 OBSERVATIONS:

The PSD is tested with a sine wave input of 50 HZ to 10 MHz. Total input voltage swing required at the difference-amplifier to carry the output of the comparator stage through

its entire swing is observed to be about 10 mV p-p.

With input signal level of about 50 mV p-p, the output of PSD approaches a step waveform satisfactorily throughout the frequency range of 50 HZ to 10 MHZ.

Fig.3.17: SCHEMATIC DIAGRAM OF POLARITY SENSING DETECTOR



## CHAPTER - 4

### MECHANICAL CONSTRUCTION AND LAYOUT

In this chapter, brief mechanical construction of housing of the printed cards and the controls have been described.

#### 4.0 PRINTED CARDS:

The distribution of 10 printed cards of 7 types used are given below:

<u>Sr.No.</u>	<u>Description</u>	<u>No. of cards used</u>
1.	Signal attenuator	1
2.	Noise generator and amplifier	1*
3.	Linear addition of signal and noise	1
4.	IF amplifier	1*
5.	Multiplier	2**
6.	Video amplifier	2**
7.	Polarity sensing detector	2**

\* The printed card has noise generator followed by a 3-stage tuned amplifier circuitry. For noise generator and amplifier at Sr.No.2, the 3rd stage of tuned amplifier has been discarded while for IF amplifier at Sr.No.4, the noise generator circuitry has not been used.

\*\* Two sets of printed cards are used for normal and quadrature channels. In printed card against Sr.No.5, a 90° phase

shifting network is incorporated which is used for quadrature channel case only.

#### 4.1 MECHANICAL CONSTRUCTION AND LAYOUT:

Printed cards against Sr.Nos.1 to 4 are housed in BOX-1 for convenience of monitoring noise and signal levels either individually or combined at IF amplifier output. The rest of the printed cards are mounted in BOX-2. The printed cards are mounted on bottom plate through spacers and fitted with screws at the bottom. The side plates cover the boxes on four sides and the middle plates shield the different printed cards. The top plate completes the structure of the box and can be fitted onto the side plates. The layouts of printed cards in Boxes-1 and -2 are shown in Figs. 4.1 and 4.2.

#### 4.2 CONTROLS:

The controls on the boxes are mounted onto the front (side) plate. Description and purpose of controls are given below:

##### 4.3.1 BOX-1: (Fig.4.1)

##### 4.3.1.1 SW-1: It is NOISE ON/OFF switch, DPST in ON (up)

position of which noise can be added to signal and in OFF (down) position, noise generator can be disconnected.

- 4.3.1.2 P-1 ; They are noise and signal level control  
&  
P-2 potentiometers respectively.
- 4.3.1.3 FTC-1 They are feed-through capacitors through which  
&  
FTC-2 +12 and -12 V supplies can be fed.
- 4.3.1.4 C-1 They are female connectors used for feeding  
&  
C-2 and obtaining the input and output signals  
respectively.
- 4.3.2 BOX-2: (Fig.4.2)
- 4.3.2.1. C-3 It is a female connector through which the signal  
(from IF amplifier output of BOX-1) can be fed  
to multipliers.
- 4.3.2.2. C-4 It is a female connector through which the  
local 60 MHZ IF can be fed to the multipliers.
- 4.3.2.3 FTC-3,5 They are feed-through capacitors through which  
FTC-4 &  
FTC-6 +5, +12 and -12V supplies respectively can be fed.
- 4.3.2.4 FTI-1 They are feed-through insulators from which the  
&  
FTI-2 normal and quadrature components of the received  
signal can be obtained.
- 4.3.2.5 FTI-3 They are feedthrough insulators through which  
and  
FTI-4 10 MHZ clock for strobing PSDs can be fed.

Fig. 4.1 : Layout of  
BOX-1

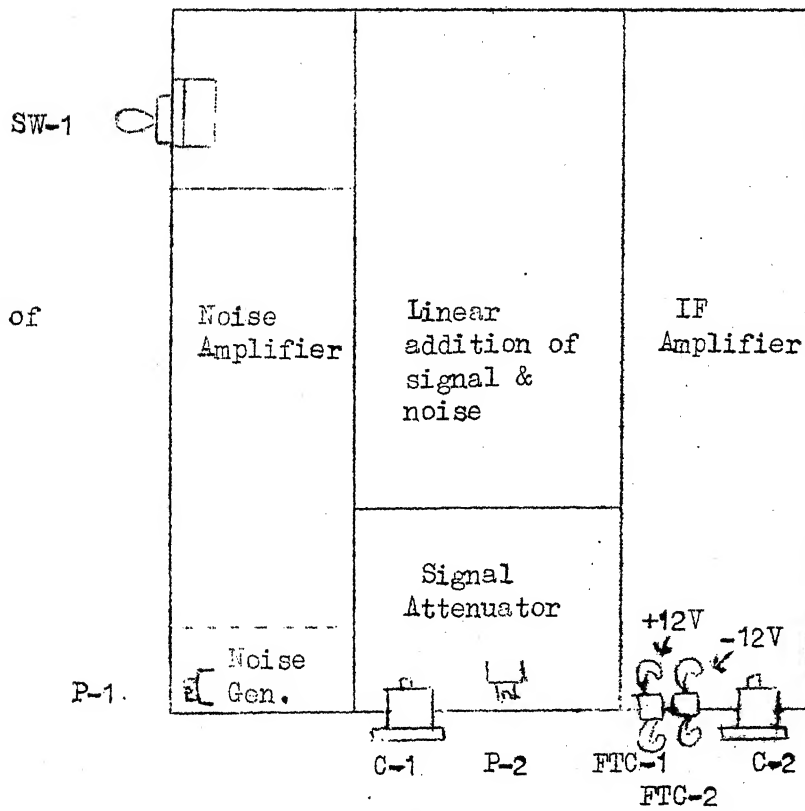
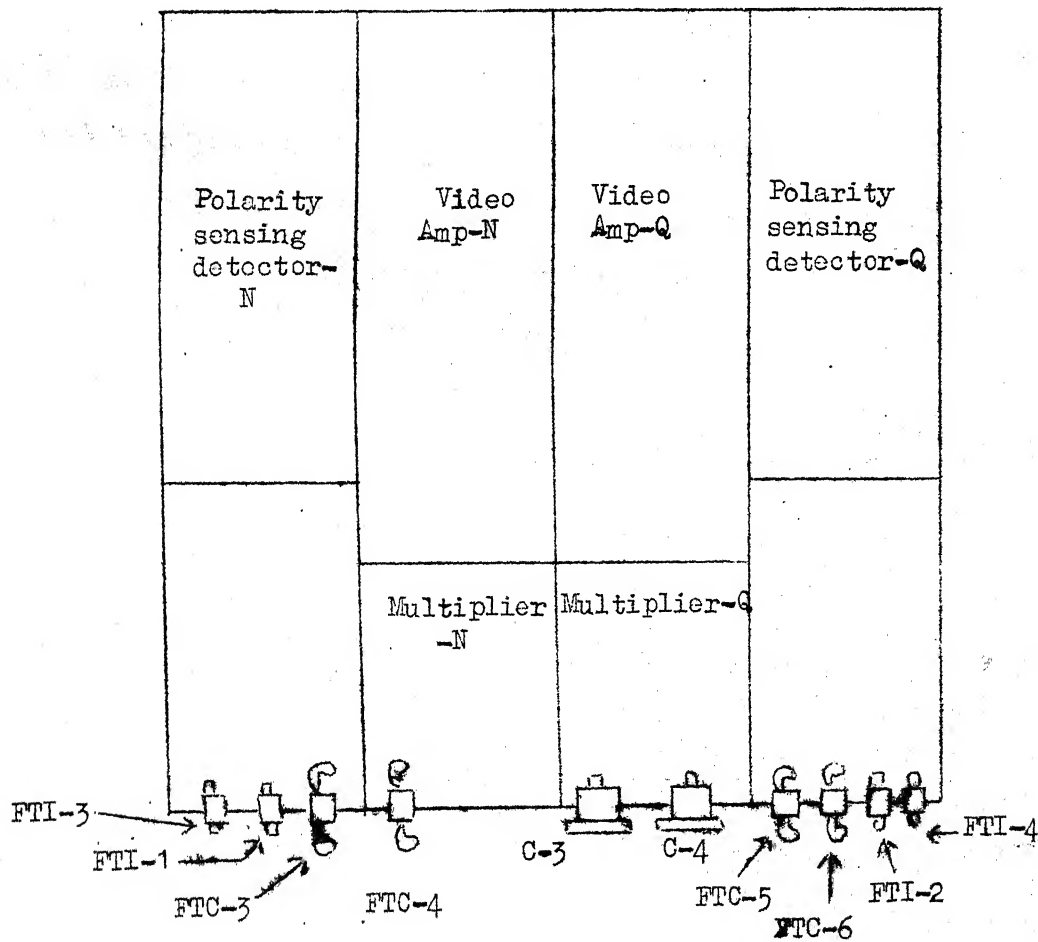


Fig. 4.2  
Layout of  
BOX-2



## CHAPTER 5

### PERFORMANCE MEASUREMENT AND CONCLUSIONS

In this chapter, a brief description of the tests conducted on the two boxes and the experimental results along with response curves have been given.

#### 5.1 Box-1: (Fig.4.1)

With final stagger-tuning of all the coupled stages, the frequency response of Signal stages constituting the signal attenuator, addition stage and IF amplifier and that of Noise stages comprising noise amplifier, addition stage and IF amplifier have been measured.

(a) Table 5.1 shows the experimental results for Signal stages as obtained with signal applied to signal attenuator and noise generator disconnected. The output is observed at the output of IF amplifier terminated into a 50-ohm load.

(b) Table 5.2 shows the results for Noise stages as observed with signal attenuator and noise generator disconnected and signal applied to noise amplifier. The observations are carried out at the output of IF amplifier terminated into a 50-ohm load.

(c) With noise generator connected, the noise level at the IF amplifier output is found to be variable from a

Table 5.1: FREQUENCY RESPONSE OF SIGNAL STAGES

Source impedance,  $R_S = 50$  ohms

Gate control voltage of signal attenuator,  $V_{GS} = 0V$

Input signal level,  $v_{in} = 48$  mV (unloaded)

24 mV (loaded)

Input signal Freq. in MHZ	IF amp. output, $v_{out}$ in mV	$\frac{v_{out}}{v_{in}}$	$\frac{v_{out}}{v_{in}}$ in dB
66	127	5.3	14.5
65	147	6.1	15.7
64	160	6.7	16.5
63	173	7.2	17.2
62	181	7.5	17.6
61	185	7.7	17.7
60	185	7.7	17.7
59	185	7.7	17.7
58	183	7.6	17.6
57	175	7.3	17.3
56	160	6.7	16.5
55	145	6.0	15.6
54	125	5.2	14.3

Centre frequency : 60 MHZ.

3dB corner frequencies: 54.2 & 65.8 MHZ

Bandwidth : 11.6 MHZ

Table 5.2 FREQUENCY RESPONSE OF NOISE STAGES

Source impedance,  $R_S = 50$  ohms.

Input signal level,  $v_{in} = 11$  mV (unloaded)

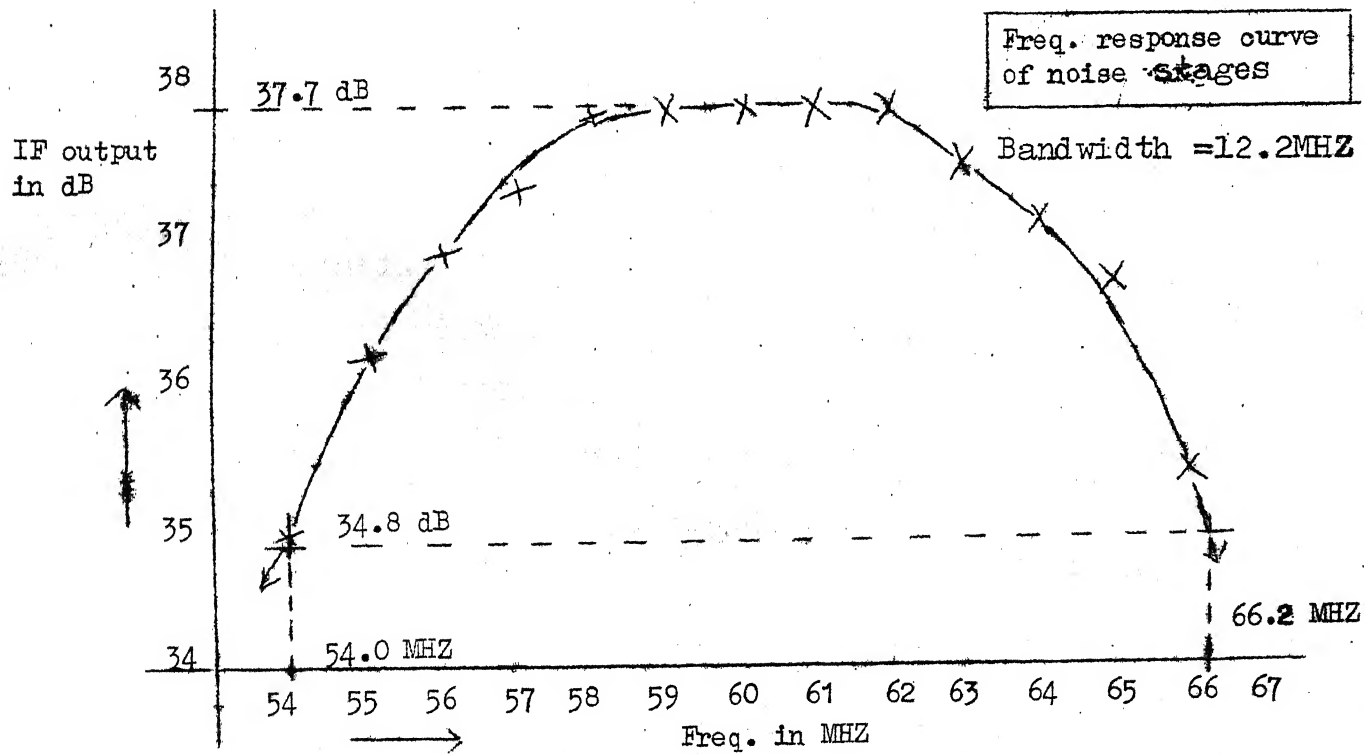
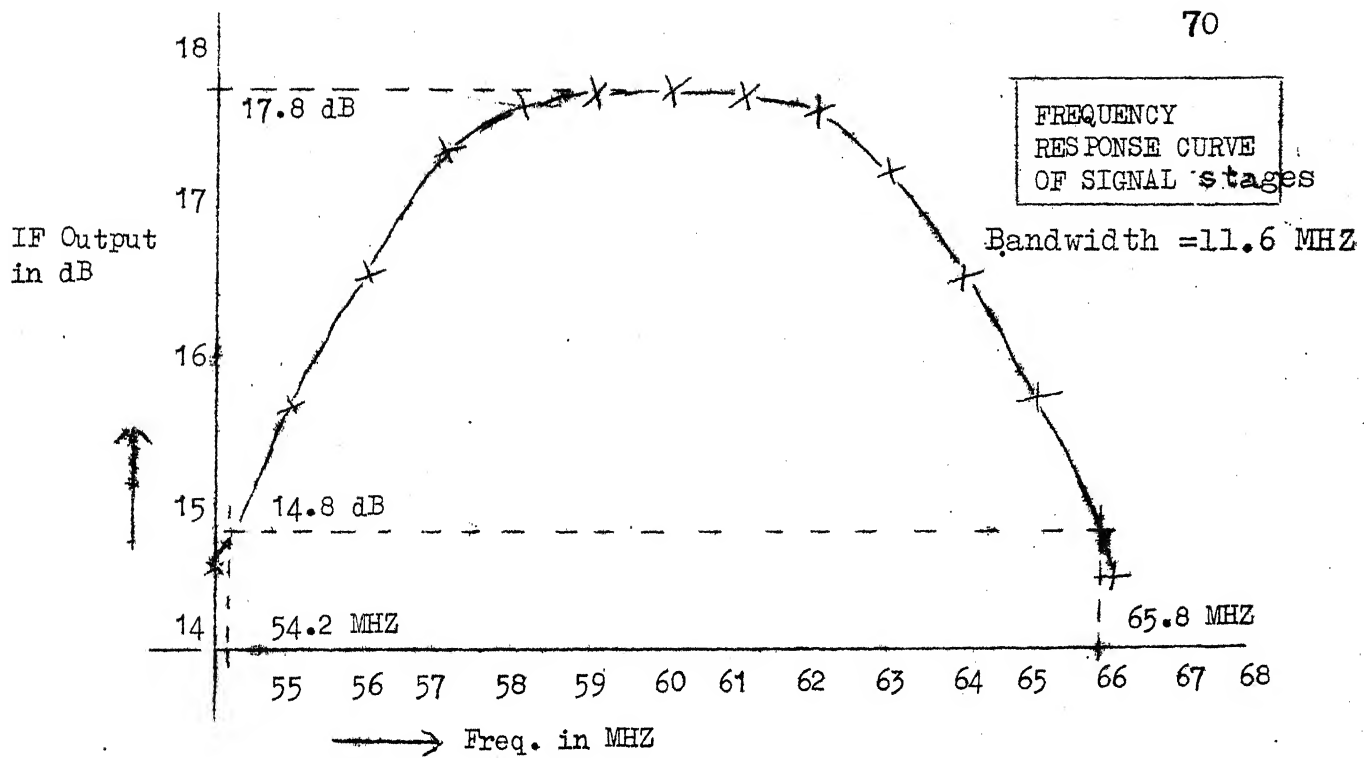
5.5 mV (loaded)

Input signal Freq. in MHZ	IF amp.out out $v_{out}$ , in mV	$v_{out}/v_{in}$	$v_{out}/v_{in}$ in dB
67	250	45.6	33.2
66	320	58.1	35.3
65	370	67.2	36.6
64	390	70.8	37.0
63	410	74.5	37.4
62	420	76.4	37.7
61	420	76.4	37.7
60	420	76.4	37.7
59	420	76.4	37.7
58	420	76.4	37.7
57	400	72.6	37.2
56	380	69.1	36.8
55	350	63.6	36.1
54	310	55.0	34.9

Centre frequency —: 60 MHZ

3 dB corner frequency —: 54 & 66.2 MHZ

Bandwidth —: 12.2 MHZ

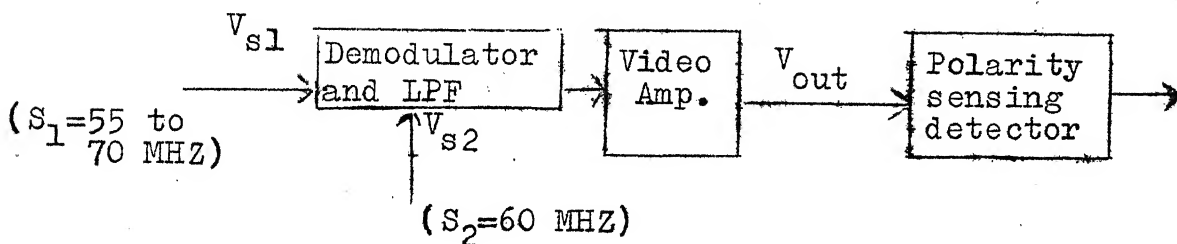


minimum of 10 mV to a maximum of 50 mV peak-to-peak.

## 5.2 BOX-2:

A brief description of the tests carried out with reference to the block diagram of Fig.5.1 is given below:

Fig.5.1



### (a) Single differential-pair multiplier using CA3028A as demodulator:

Testing of Box-2 is carried out by applying 60 MHz signal to the voltage-gain controlling  $S_2$ -input (see 'Multiplier', section 3.5) and 55 to 70 MHz variable frequency signal to the differential  $S_1$ -input of the multiplier stage from two different VHF oscillators.  $V_{s1}$  and  $V_{s2}$  are the voltage levels of  $S_1$  and  $S_2$  respectively and the voltage levels of the video component after amplification are observed as  $V_{out}$  for different frequencies of  $S_1$  ranging from 55 to 70 MHz in steps of 2.5 MHz. The results are tabulated in Table 5.3 from which it is observed that (since the video amplifier is found to have bandwidth of 10 MHz) the differential pair multiplier using CA3028A has bandwidth limitation of 5.7 MHz.

Table 5.3

$$V_{s1} = 120 \text{ mv}$$

$$S_1 = 55 \text{ to } 70 \text{ MHz}$$

$$V_{s2} = 275 \text{ mv}$$

$$S_2 = 60 \text{ MHz}$$

$S_1$	55 MHZ	57.5 MHZ	60 MHZ	62.5 MHZ	65 MHZ	67.5 MHZ	70 MHZ
$V_{out}$	400 mv	470 mv	520 mv	465 mv	390 mv	290 mv	250 mv

(b) Double balanced mixer (Ring demodulator) using DBM-1 (ANIDUS make)

The differential-pair multiplier using CA3028A is replaced by double balanced mixer (Ring demodulator) and with the experimental set-up as shown in Fig.5.1, the observations are made at the output of the demodulator. The results are tabulated in Table 5.4 showing the better performance of the ring demodulator over that of differential pair multiplier.

Table 5.4

$$V_{s1} = 250 \text{ mv}$$

$$S_1 = 55 \text{ to } 70 \text{ MHz}$$

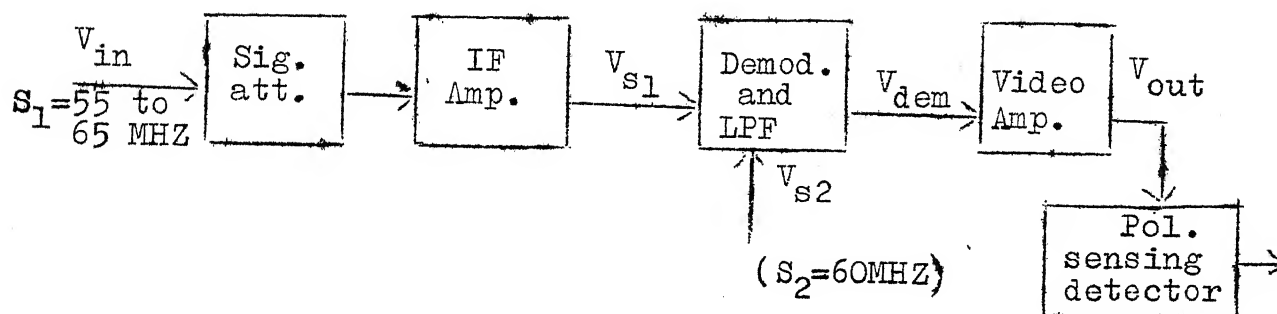
$$V_{s2} = 500 \text{ mv}$$

$$S_2 = 60 \text{ MHz}$$

$S_1$	55 MHZ	57.5 MHZ	60 MHZ	62.5 MHZ	65 MHZ	67.5 MHZ	70 MHZ
Demod. output	200 mv	200 mv	200 mv	200 mv	200 mv	195 mv	190 mv

5.3 Testing of the overall fabricated part constituting Boxes-1 and -2 is carried out, the description of which with reference to block diagram of Fig.5.2 is given below.

Fig.5.2



The signal  $S_1$  of variable frequency from 55 to 65 MHz is applied to the signal attenuator and the IF amplifier output is coupled to the demodulator, the other input of which being  $S_2$  of 60 MHz

- $V_{in}$  : Level of input signal  $S_1$  to signal attenuator
- $V_{s1}$  : IF amplifier output
- $V_{s2}$  : Level of  $S_2$
- $V_{dem}$  : Level of video component at the demodulator output
- $V_{out}$  : Video amplifier output

(a) The response of Box-1 under loaded conditions is measured as a function of frequency. The experimental results are given in Table 5.5 and the corresponding  $V_{s1}$  vs freq. plot in Fig.5.3 showing the IF amplifier output  $V_{s1}$  for different frequencies of  $S_1$  ranging from 55 to 65 MHz.

The bandwidth of signal stages (signal attenuator, addition stage and IF amplifier) under loaded conditions is found to be 10 MHz.

Table 5.5

$$V_{in} = 60 \text{ mv}$$

$S_1$ in MHZ	65	63	61	60	59	57	55
$V_{s1}$ in mv	198	232	250	257	255	238	204

(b) Differential-pair multiplier using CA3028A as demodulator:

Voltage levels of the video component  $V_{out}$  at the video amplifier output are measured for different frequencies of  $S_1$  ranging from 55 to 65 MHz in steps of 2 MHz. The results are tabulated in Table 5.6 from which it may be concluded that the differential pair multiplier using CA3028A limits the bandwidth of the fabricated part of the system to 3MHz. The plot of  $V_{out}$  vs. frequency is shown in Fig.5.4.

Table 5.6

$S_1$  : 55 to 65 MHz

$S_2$  : 60 MHz

$V_{in} = 60 \text{ mv}$

$V_{s2} = 360 \text{ mv}$

$S_1$ in MHz	55	57	59	60	61	63	65
$V_{out}$ in mv	75	97	126	137	126	99	78

(c) The observations made with double balanced mixer are recorded in Table 5.7 showing the bandwidth of the system to be more than 10 MHz (about 12 MHz). The frequency response curve is plotted in Fig.5.5.

Table 5.7

$$V_{in} = 60 \text{ mv}$$

$$V_{s2} = 1.2 \text{ v}$$

$S_1$ in MHZ	55	57	59	60	61	63	65
$V_{dem}$ in mv	200	240	255	260	250	235	195

#### 5.4 LIMITATIONS:

- (a) Noise level control is not sensitive.
- (b) Differential pair multiplier limits the bandwidth of the system to 3 MHz.
- (c) High-frequency rejection at the demodulator output is poor.

#### 5.5 SPECIAL FEATURES:

(a) Signal Attenuator using FET as a voltage-controlled resistor provides (i) continuous attenuation range and (ii) flexibility of band-width adjustment with suitable drain and source resistances shunting the input and output tank circuits respectively.

(b) Tunability to various frequencies:

With proper stagger-tuning of the tuned circuits,

the fabricated part can be used for operation with IF frequency of any value between 60 MHz with overall bandwidths of signal and noise stages being 10 MHz each.

(c) Bandwidth of the video Amplifier can be increased (to about 20 MHz) without any high-frequency peaking networks.

#### 5.6 SUGGESTIONS FOR IMPROVEMENTS:

(a) An attenuator stage (similar to that used for signal attenuation) at the output of noise amplifier provides a fine control of noise level.

(b) A calibrated meter/indicator (at the output of IF amplifier) facilitates the monitoring of signal and noise level

(c) CE-to-CB cascode circuits between each multiplier and IF amplifier gives better isolation between the input and outputs of multiplier stages.

(d) A double balanced mixer (A ring demodulator) type DBM-1 (ANIDUS make) in the place of single differential-pair multiplier using CA3028A gives required overall bandwidth of 10 MHz.

(e) A two-stage Butterworth low-pass filter at the output of multiplier stage can provide better high-frequency rejection

(f) Video amplifier can be replaced by one or two more stages of difference-amplifier before the comparator circuit.

Fig.5.3

77

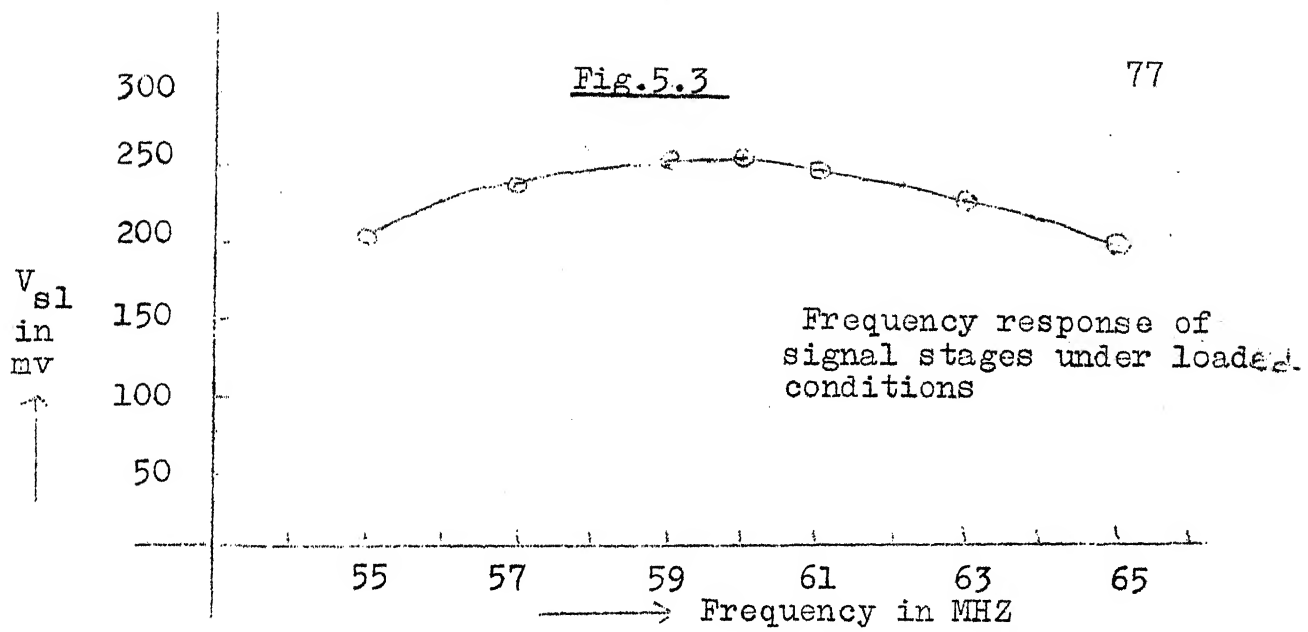


Fig.5.4

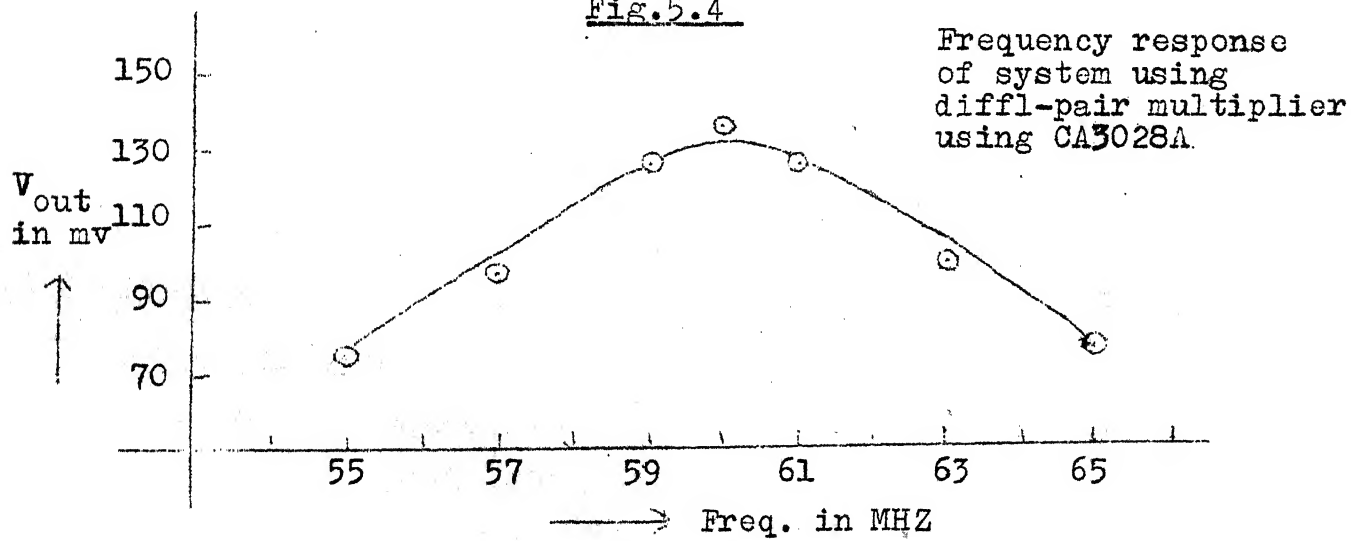
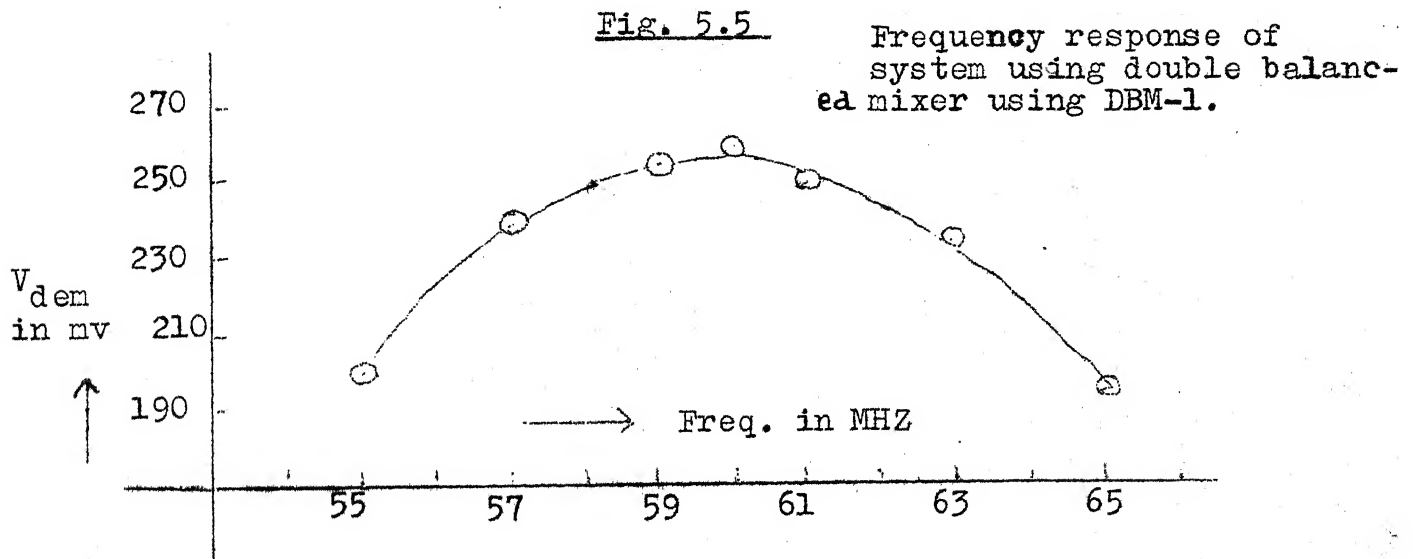


Fig. 5.5



APPENDIX-ABRIEF MANUFACTURER'S SPECIFICATIONS OF DEVICES

Type	Max. Ratings				Ele. characteristics		
	$V_{CB}$	$V_{CES}$	$V_{BE}$	$I_C$	Conditions	$h_{FE}$	$f_T$
(1) 2N3324 PNP, Ge	35V	35V	3V	100ma	$V_{CE}=10V$ , $I_C=3ma$	30 to 200	200 to 600 MHz
(2) 2N918 NPN, Si	30V	15V	3V	50ma	$V_{CE}=10V$ $I_C=10ma$	20	960 MHz
(3) 2N3563 NPN, Si	30V	12V			$I_C=8ma$	20 to 200	600 MHz

(4) BFW10: (N-channel, silicon, JFET)

Gate-source voltage (open drain),  $-V_{GS0} \max = 30V$

Feedback capacitance at 1 MHz ( $V_{GS}=0, V_{DS}=15V$ ),  $-C_{re} < 0.75pf$

Transfer admittance (common source) ( $V_{GS}=0, V_{DS}=15V$ ),

$$Y_{FS} > 3.2 \text{ m mhos}$$

(5) SZ213: (Silicon epoxy, zener diode)

Nominal reference voltage,  $V_{br} = 8.2V$

Max. dissipation at 25°C = 250mw

(6) CA3028A: (Linear IC)

It is a differential/cascode amplifier for operation at frequencies DC to 120 MHz.

Elec. characteristics (at  $f=10.7MHz, V_{CC}=+9V$ )

	Cascode	Diff. Amp
$Y_{11}$	$0.6 + j 1.6 \text{ m}\Omega$	$0.5 + j 0.5 \text{ m}\Omega$
$Y_{12}$	$0.0003 - j 0$	$0.01 - j 0.0002 \text{ m}\Omega$
$Y_{21}$	$99 - j 18$	$-37 + j 0.5$
$Y_{22}$	$0 + j 0.08$	$0.04 + j 0.23$

REFERENCES

1. "Field effect transistors", WALLMARK & JOHNSON, Prentice Hall.
2. "Wave generation & Shaping", STRAUSS, McGraw Hill.
3. "Low Frequency white Gaussian Noise Source", MULLICK, SINGH & SANGHI, J of ITE; 1971, Vol.17, No.3, pp.98-102.
4. "Radio Handbook", W.I. ORR.
5. "Principles & Applications of Semiconductors & Circuits", COUGHLIN, Prentice Hall.
6. "Reference Data for Radio Engineers", ITT Corp., 1956.
7. "Transistor Circuit Design", TEXAS Staff, McGraw Hill.
8. "Transistor Circuit Engineering", COCHRAN, Macmillan.
9. "Troposcatter multipath analyzer", BARROW, Sylvania Ele. Systems, Rpt. No.ACSO-TR-01-70, 1970.
10. "Indirect Atmospheric Measurements using RAKE Tropo-scatter Tech.- Part I: RAKE Troposcatter Tech.", BARROW, ABRAHAM, COWAN & GALLANT, Proc. IEEE, Vol.57, No.4, April 1969, pp 537-551.
11. "Tropospheric-scatter propagation tests using RAKE Receiver", BARROW, ABRAHAM, STEIN & BITZER, Sylvania Ele. Systems, Rpt. No.461, 1965.
12. "Communication Systems & Techniques", SCHWARTZ, BENNET & STEIN, McGraw Hill.
13. "Communication Circuits: Analysis & Design", CLARKE & HESS, Addison-Wesley.
14. "Design Manual for Transistor Circuits", CARROLL, McGraw Hill.
15. "Pulse, digital & switching waveforms", MILLMAN & TAUB, McGraw Hill.
16. "Communication Engineering", EVERITT & ANNER.
17. "Semiconductors: Physics, Devices and Circuits", CIROVIC, Prentice Hall.